Available online at www.sciencedirect.com
ScienceDirect
Applied Catalysis B: Environmental 81 (2008) 161–181
APPLIED CATALYSIS B: ENVIRONMENTAL
www.elsevier.com/locate/apcatb

Selective catalytic reduction of NO by H_2 in O_2 on Pt/BaO/Al_2O_3 monolith NO_x storage catalysts☆

Robert D. Clayton, Michael P. Harold *, Vemuri Balakotaiah *

Department of Chemical & Biomolecular Engineering, University of Houston, Houston 77204-4004, TX, United States

Received 31 August 2007; received in revised form 20 November 2007; accepted 30 November 2007
Available online 8 December 2007

Abstract

Comprehensive steady-state experiments of the selective catalytic reduction of NO on a series of Pt, Pt/BaO, and BaO monolithic catalysts have been carried out to evaluate the light-off, NO_x conversion and product distribution features as a function of the feed composition, temperature and catalyst composition. The reaction between NO and H_2 produces a mixture containing N_2O, NH_3, and N_2, the composition of which is a function of the catalyst temperature and NO/H_2 ratio in the feed. NO inhibits the reaction at low temperatures as revealed by light-off temperature and supporting kinetic data. NO_x conversions were found to be complete at space velocities below 90,000 h^{-1} and above 100 °C for Pt loadings exceeding 1.27 wt.%. At low temperature and O_2 concentration the NO–H_2 reaction mainly produces N_2O and is positive (negative) order in H_2 (NO). The light-off temperature of the NO–H_2 system is dictated by these kinetics as well as the Pt loading. Complementary theoretical analyses elucidate selected kinetic trends and the effect of Pt loading on the conversion versus temperature trends. The NO–H_2–O_2 data are interpreted with a phenomenological reaction network model. Particular attention focused on the production and consumption of ammonia, a problematic byproduct during conventional NO_x storage and reduction (NSR). NH_3 is a major product under O_2 deficient conditions typical of the rich pulse in NSR, while N_2 and N_2O are the main products at higher O_2 concentrations (lean conditions). NH_3 oxidation ignites on Pt catalysts at 170–180 °C; in the ignited state a mixture of N_2, NO, NO_2 and N_2O is produced, the composition of which is sensitive to the NH_3/O_2 feed ratio and temperature. Experiments involving a feed containing H_2, NH_3, and NO show complete H_2 conversion and negligible net NH_3 conversion. For temperatures exceeding 150 °C an equimolar mixture of the three components results in complete NO reduction by H_2 with negligible conversion of NH_3. The decomposition of NH_3 is observed above 330 °C but is kinetically inhibited by H_2. A comparison of the Pt and Pt/BaO catalysts reveals similar steady-state behavior. The BaO catalyst exhibited a non-negligible but lower activity and a different product distribution than the Pt and Pt/BaO catalysts.

Keywords: NO_x; Hydrogen; Platinum; Barium; Selective catalytic reduction; NO_x storage and reduction; Lean NO_x trap

1. Introduction

The production of ground level ozone caused by the emission of NO_x from lean burn and diesel engines is the main driving force for the active research in lean NO_x reduction. Compression ignition engines fueled by diesel are more efficient than spark ignition engines fueled by gasoline, but the NO_x is contained in excess O_2, which undermines the reduction of NO_x in the conventional three-way catalytic converter. Several NO_x reduction technologies are under vigorous development, including exhaust gas recirculation (EGR) with advanced particulate traps, selective catalytic reduction (SCR) with ammonia or urea, steady-state SCR with hydrocarbons (HC), and NO_x storage and reduction (NSR).

The focus of the current study is on NSR which is a periodic catalytic process used to convert NO_x to N_2. The catalytic

☆ *Disclaimer*: This report was prepared as an account of work sponsored by an agency of the United State Government. Neither the United States Government nor any agency thereof, nor any of their employees, makes any warranty, express or implied or assumes any legal liability or responsibility for the accuracy, completeness, or usefulness of any information, apparatus, product, or process disclosed, or represents that its use would not infringe privately owned rights. References herein to any specific commercial product, process, or service by trade name, trademark, manufacturer, or favoring by the United States Government or any agency thereof. The views and opinions of authors expressed herein do not necessarily state or reflect those of the United States Government or any agency thereof.

* Corresponding authors.
E-mail addresses: mharold@uh.edu (M.P. Harold), bala@uh.edu (V. Balakotaiah).

0926-3373/$ – see front matter © 2007 Elsevier B.V. All rights reserved.
doi:10.1016/j.apcatb.2007.11.038

Nomenclature

C	concentration (mol/cm^3)
C_f	dimensionless feed concentration
D	molecular diffusivity (cm^2/s)
D_{eff}	effective diffusion coefficient within the washcoat pores (cm^2/s)
Da_o	Damkohler number
Da_o^*	Damkohler number at the reference temperature and concentration
E	activation energy (kJ/mol)
F	feed rate (mol/s)
k_c	mass transfer coefficient (cm/s)
k_i	rate constant for step i
k_v	first-order rate constant (s^{-1})
K	adsorption equilibrium constant
L	length of monolith (cm)
P	transverse Peclet Number
P_i	partial pressure of specie i
P_Ω	perimeter of the channel (cm)
Pe_x	Peclet number
r	reaction rate (mol/s cm^3)
R	universal gas constant, 8.314×10^{-3} (kJ/mol K)
R_Ω	hydraulic radius (cm)
S	selectivity (%)
S_N	Stoichiometric number
Sh	Sherwood number
T	temperature (°C)
u_f,	mean fluid velocity (cm/s)
$\dot{V}$	volumetric flow rate (cm^3/min)
$V_{w.c.}$	volume of the washcoat (cm^3)
X	conversion (%)

Greek letters

α_1	first numerical constant
δ_w	effective washcoat thickness (cm)
ε	porosity of washcoat
ϕ	Thiele modulus
γ	dimensionless activation energy
μ_1	first eigenvalue
θ	fractional coverage of surface species
τ	tortuosity factor

Subscripts

avg.	weighted average
i	index of species
in	inlet
o	reference conditions
out	outlet
s	surface

process consists of two stages which take place in the ''lean NO_x trap'' (LNT) comprising a bifunctional monolithic catalyst of precious metals (Pt, Rh, Pd) used for NO oxidation and reduction, and an alkaline earth metals in the form of an oxide or carbonate (Ba, K, Sr, etc.), used to store NO_x. In the first stage NO is oxidized on Pt to NO_2 which then reacts with the alkaline earth compound forming nitrites and nitrates. Before an unacceptable amount of NO_x breaks through, the second stage is commenced. This stage consists of a short, rich ''purge'' of a reductant (HC, CO, H_2, NH_3) during which stored NO_x is reduced. The length of the rich pulse is determined by the amount of NO_x stored. If the pulse is too short, the regeneration of the catalyst will be incomplete. If the pulse is too long the reductant will break through and undesirable byproducts may be produced (such as NH_3 when H_2 is a reductant). In NO_x traps Pt is very effective in oxidizing NO to NO_2, which enables the storage process to proceed. Rather high loadings of Pt (1–2 wt.%) are needed to efficiently store and reduce NO_x in comparison to the typically much lower loadings (<0.2%) used in TWC converters. The effectiveness of the NO_x trap improves with increasing Pt loading up to ca. 2%, but the incremental improvements diminish at Pt loadings exceeding 2% [1].

The main aim of NSR technology is to achieve high NO_x conversion while maintaining a high selectivity towards N_2 and not incurring a large fuel penalty. The NSR catalyst must be able to withstand the intermittent high temperature desulfations and prolonged use (e.g. >100 K miles in a lean burn gasoline vehicle and >400 K miles in a heavy duty diesel vehicle). These are daunting obstacles to NSR commercialization.

The catalytic reduction of NO on supported noble metals was studied extensively in the 1970s and 1980s during the development of the TWC converter. There are many similarities between the reduction of NO_x in the TWC converter in the exhaust of stoichiometric, spark ignition vehicles and the regeneration stage of NSR. Similar to NO_x traps, the main precious metal used in TWC converters is Pt. Another similarity is the reductant types, which include exhaust hydrocarbons, CO, and H_2. Both processes encounter time-varying feeds because of the inherent transient nature of vehicle operation. The obvious difference is that lean NO_x trap is deliberately operated as a periodic process in order to react away stored NO_x, while the TWC converter can operate close to steady-state conditions. Notwithstanding this difference, knowledge of the steady-state behavior of representative Pt, Pt/Ba, and Ba catalysts is essential for understanding the more complex two-step storage and reduction process. This is the focus of the current study.

It is instructive to highlight the main findings of previous studies which focused on the use of H_2 as a reductant and Pt as the precious metal catalyst. Kobylinski and Taylor [2] compared the reduction of NO with H_2, CO, and an equimolar mixture of CO/H_2 over supported Pd, Pt, Rh, and Ru catalysts. They determined the order of activity to be Pd > Pt > Rh > Ru when H_2 was the reductant. When CO or CO/H_2 was used the order was reversed because CO was found to strongly inhibit NO reduction on Pt and to a much lesser extent on Rh, while enhancing the activity of Ru. Muraki and Fujitani [3] observed a similar ranking of Pt > Pd > Rh for the reduction of NO with H_2 and NH_3 and the opposite order for the reduction with CO. Schlatter and Taylor [4] found that adding Pt or Pd to the Rh supported catalyst enhanced the oxidation capabilities, but

resulted in a large increase in the production of NH_3 under reducing conditions. The formation of ammonia was minimized by isolating the metals on different supports with Rh upstream of Pt or Pd, while maintaining high activity towards NO reduction. Hirano et al. [5] determined the order of activity and selectivity to N_2 for different Pt, Rh, and Pt–Rh alloy catalysts. They concluded that the activity and selectivity of the different metals was determined by the relative concentrations of N, H, and NO on the surface. Stenger and Hepburn [6] noted that the intrinsic activity of NO reduction by H_2 was Pt > Pd > Rh. The reaction rates for the formation of N_2, N_2O, and NH_3 were fit to a simplified Langmuir-Hinshelwood model. Hecker and Bell [7,8] studied the kinetics of the NO/H_2 and NO/H_2/CO reaction over Rh/SiO_2 and fit their measured rates to a power law expression. Papapolymerou et al. [9] also studied the kinetics of the NO/H_2 reaction over polycrystalline wires and foils and interpreted their results with a Langmuir-Hinshelwood based mechanism. Klimisch and Taylor [10] showed that Pt/Al_2O_3 produced NH_3 as the primary product for feeds containing NO and H_2 system. Pt was reported to be active below 200 °C for the same reaction system [10,11]. Otto and Yao [12] and Yao et al. [13] both observed two distinct phases of Pt, a dispersed and a particulate phase. The particulate phase was shown to be more active during NO reduction with H_2 than the dispersed phase. This was attributed to the need for multiple Pt sites (Pt-clusters) for the chemistry to occur [12]. The dispersed phase has also been shown to have a stronger interaction with the γ-Al_2O_3 support than the particulate phase [13].

The reduction of nitric oxide with H_2 over noble metal catalysts produces a complex mixture of N_2, N_2O, and NH_3 [5,8]. NH_3 is an undesired byproduct due to its toxicity and noxious odor, and therefore must be minimized in the exhaust. Several groups have studied the decomposition of NH_3 and have shown that H_2O and H_2 inhibit the NH_3 decomposition rate [11,14,15]. H_2O is believed to retard NH_3 decomposition by reducing the adsorption of NH_3 since NH_3 and H_2O have similar chemisorption behavior [14]. The CO/NO/H_2O system is also known to form NH_3 in the absence of H_2. H_2 is produced by the water gas shift reaction (WGS), which then reacts with NO [14]. Kobylinski and Taylor [2] observed the inhibition of NH_3 decomposition by addition of CO to a feed stream of NH_3/Ar. Similarly, in the absence of H_2O, when CO is added to the NO/H_2 system over Pt, the NH_3 formation decreased [16]. Stenger and Hepburn [6] postulated that N_2O is the main product formed on Pt from the H_2/NO reaction and NH_3 is a secondary product formed from the reaction of N_2O with H_2. NH_3 was also observed as an intermediate in the NO/H_2 system; NH_3 is formed via NO reduction and then decomposes to N_2 rapidly above 425 °C [11].

The reduction of NO by NH_3 may be an important reaction during NO_x storage and reduction. Recent studies have reported that ammonia serves as a hydrogen carrier and reduces stored NO_x on Pt/Ba catalysts [17]. Earlier studies reported that NH_3 reacts selectively with NO in the presence of O_2 on noble metals [18–21] and a variety of mixed metal oxides, notably vanadia/titania based catalysts [22,23]. The reaction has been shown to produce N_2O both in the absence of O_2 [24,25] and presence of O_2 [18,26]. Otto et al. [25,27] studied the NO/NH_3 reaction by nitrogen-15 isotope labeling. They reported that N_2O is predominantly formed by the reaction of adjacent NO molecules, while N_2 is formed by the reaction of adsorbed NH_3 and NO. Gland and Korchak [28] determined the rate limiting step of the NO/NH_3 reaction to be the reaction between an adsorbed fragment of NH_3 and an adsorbed NO molecule. They modeled the rate expression using a single site Langmuir-Hinshelwood kinetic model similar to that of Otto et al. [25,27]. The model comprises the associative adsorption of NO and dissociative adsorption of NH_3.

Finally, the oxidation of ammonia on Pt may be encountered under some conditions during NO_x storage and reduction. Ammonia oxidation by O_2 on precious metal catalysts has been extensively studied (too numerous to list here). The oxidation of ammonia on Pt(90%)–Rh(10%) alloys (woven into gauzes) is one of the steps in the production of nitric acid, one of the large-scale processes in the chemical industry. Approximately, 10–12% NH_3 is fed in air with a yield to NO strongly dependent on the pressure and temperature (1.7–6.5 bar and 810–940 °C). Similar to the reaction between NH_3 and NO, the reaction between NH_3 and O_2 forms N_2O at low temperatures [25,27,29]. Ostermaier et al. [29] also observed the selectivity to N_2O increasing with increased amounts of O_2 at low temperatures.

Recently, technological advances have shown that NH_3 formed during the regeneration of the NO_x trap can also be beneficial if the NO_x trap is used in conjunction with a NH_3-SCR catalyst downstream [30–33]. DaimlerChrysler is presently releasing this technology to the U.S. through Mercedes in the E320 ‘‘Bluetec’’ model. This model is able to achieve the ‘‘Tier 2 Bin 8’’ emission levels required for 45 of the 50 states. The exhaust aftertreatment system includes a diesel oxidation catalyst (DOC) followed by the NO_x adsorption catalyst (NAC), diesel particulate filter (DPF), and an SCR catalyst. An engine management strategy is used to periodically produce rich exhaust conditions that will reduce the NAC, producing N_2 and NH_3. The NH_3 stores downstream on the SCR catalyst and reacts further with NO_x that breaks through from the NAC catalyst during the subsequent lean cycle [30]. Hemingway [31] and Hu [32] proposed using an onboard partial oxidation reformer upstream of the Lean NO_x Trap (LNT) to produce reductants (H_2 and CO) to reduce the stored NO_x in the LNT producing N_2 and NH_3. The NH_3 will further react downstream in the SCR reducing NO_x that was unable to be reduced in the LNT. Morita et al. [33] proposed a slightly different set up in which the NH_3-SCR and LNT are conjoined in a bi-layered catalyst. The underlying layer consists of Pt supported on CeO_2 (storage) and the upper layer has a transition metal ion-exchange zeolite as a solid acid (NH_3-SCR). Morita et al. [33] claimed that CeO_2 stores NO_x better than BaO at low temperatures (<250 °C) and also promotes excellent activity for the WGS reaction at low temperatures.

The objective of the current study is to conduct a comprehensive study of the steady-state reaction between NO and H_2 in the presence of O_2 on Pt/BaO catalyst. We report

conversion and selectivity for several of the chemistries that occur during NO_x storage and reduction. The data are analyzed with a phenomenological model of the underlying surface chemistries and compared to the results of previous studies. Finally, implications of the findings with regards to NO_x storage and reduction are discussed and some theoretical analyses are carried out to elucidate some of the trends.

2. Experimental

2.1. Catalyst samples

Monolith catalysts used in this study were provided by BASF Catalysts LLC (formerly Engelhard Corporation; Iselin, New Jersey). Larger cylindrical cores ($D = 3.8$ cm, $L = 7.6$ cm) were cut using a dry diamond saw to smaller, nearly cylindrical shapes; two sizes were used in the current study: $D \sim 0.8$ cm, $L = 2$ cm; $D \sim 0.8$ cm, $L = 0.67$ cm. For this diameter, the monolith contained 28 channels. The samples contained varying amounts of Pt and BaO on a γ-alumina washcoat support on a cordierite structure (~62 channels/cm^2). Based on average washcoat loadings provided by BASF, the mass of washcoat (m_{wc}) on each monolith piece was estimated to be 0.101 and 0.034 g, respectively. The compositions and properties of the catalysts are given in Table 1 (analyses conducted by BASF). The monoliths were wrapped in Fiberfrax® ceramic paper that had been heat-treated and then placed in a quartz tube flow reactor. The methods used to measure catalyst properties are described in a previous publication [1].

2.2. Flow reactor set-up

The experimental set-up is similar to the one used in a previous study [1]. The effluent from the flow reactor was analyzed downstream with a FT-IR spectrometer and O_2 analyzer. The species monitored by the FT-IR included NO, NO_2, N_2O, NH_3, and H_2O. Temperatures were monitored with three 1/16-in. diameter K-type stainless steel thermocouples. The thermocouple utilized for these experiments measured the catalyst temperature (T_c) which was positioned within an internal monolith channel at the approximate mid-point of the monolith (radial and axial). The gas feed (T_f) and outlet (T_o) temperatures were also monitored 1 cm before the catalyst and 1 cm after the catalyst, respectively. Some heat losses occurred in this system due to the rather small diameter of the monolith, so the data do not truly represent adiabatic operation. However, our calculations of the heat transfer characteristics of the reactor indicated that the variation of temperature along the length of the catalyst was negligible under non-reaction flow conditions because of the short length relative to the length of the furnace heating zone. For some of the experiments a quadrupole mass spectrometer (QMS) was used to measure N_2 and H_2 concentrations. The QMS was tied into the effluent line approximately 0.6 m downstream of the FT-IR.

2.3. Catalyst aging

Prior to testing each catalyst, an aging process was imposed in order to stabilize the catalyst activity so that experiments could be compared without large activity changes over prolonged periods of time on stream. The catalyst was aged at 650 °C in 3% O_2 and 6.5% H_2 for 3.5 h. Periodic experiments were run to evaluate the activity level of the catalyst. The activity test revealed that deactivation occurred for long exposures to temperatures exceeding 500 °C. Therefore, experiments in which the catalyst temperature exceeded 500 °C were avoided.

2.4. BaO activation

The fresh BaO catalysts were activated at 600–650 °C in different atmospheres (3% O_2 and 6.5% H_2, 500 ppm NO and 1250 ppm H_2, and Ar only). The times and temperatures for activation were varied between 1 and 4 h and 400–650 °C.

2.5. Steady-state experiments

The steady-state experiments were carried out by first flowing N_2 and then adding the reactive gases to the reactor. In some cases the order of reactants was varied to probe different steady-states of the catalyst. The feeds employed in this study did not contain CO_2 or water; the effects of these exhaust components will be investigated once a complete understanding of the simpler feed is secured. Most of the experiments involved measuring the product distribution as a function of the monolith temperature by systematic variation in the furnace power. This procedure was followed in order to span the catalyst temperature range, usually from 30 to 500 °C. In the experiments in which the FT-IR and O_2 analyzer were exclusively used to measure the effluent composition, the N_2 and H_2 effluent concentrations were determined by overall N and H balances. The 2 cm long monolith samples were used for all of the experiments except for the H_2/NO space velocity tests,

Table 1
List of monolith catalysts used and their properties

Sample	Pt (wt.%)	BaO (wt.%)	Pt dispersion %	Pt area (m^2/g)	Pt particle size (nm)	BET area (m^2/g)
B0	0	16.7	N/A	N/A	N/A	107
B1	0.32	16.6	39.8	0.31	2.85	111
B2	1.27	16.5	33	1.04	3.43	109
B3	2.2	16.3	21.9	1.19	5.18	116
B4	3.71	16	34.7	3.18	3.26	107
A3	2.63	0	20.3	2.21	5.59	–

which used the 0.67 cm long samples. The length of the catalysts were decreased to 1/3 (0.67 cm) of the original length (2 cm) in order to increase the gas hourly space velocity (GHSV), which was varied from 90,000 to 360,000 h^{-1} in these particular experiments. The GHSV is based on the catalyst volume and is defined as GHSV = F/V_m where F is the volumetric flow rate (std. cm^3/h) and V_m is the monolith volume (cm^3). Conversion has the standard definition. Selectivities reported here are based on NO_x reacted with a N atom basis.

3. Experimental results

3.1. Anaerobic NO_x reduction

In order to better understand the H_2 and NO chemistry on Pt/BaO/Al_2O_3, experiments were carried out with 500 ppm of NO and varied amounts of H_2 in the absence of O_2 (anaerobic conditions) on a BaO/Al_2O_3 catalyst at 360 °C (Fig. 1a). Identical reaction conditions were used for $Pt/BaO/Al_2O_3$ (Fig. 1b) and Pt/Al_2O_3. Similar results for the Pt/Al_2O_3 catalyst were reported elsewhere [34]. Anaerobic conditions are encountered at the end of rich pulse (containing no oxygen) that is of sufficient duration under cycling conditions; i.e. when depletion of gas phase O_2 has occurred. [Remark: NSR carried out for lean burn gasoline vehicles typically contains less than 1.5% O_2 while in diesel applications the O_2 concentration can be as high as 5–10%.]

The dependence of the NO_x conversion and product selectivities on the H_2/NO ratio is shown in Fig. 1a and b.

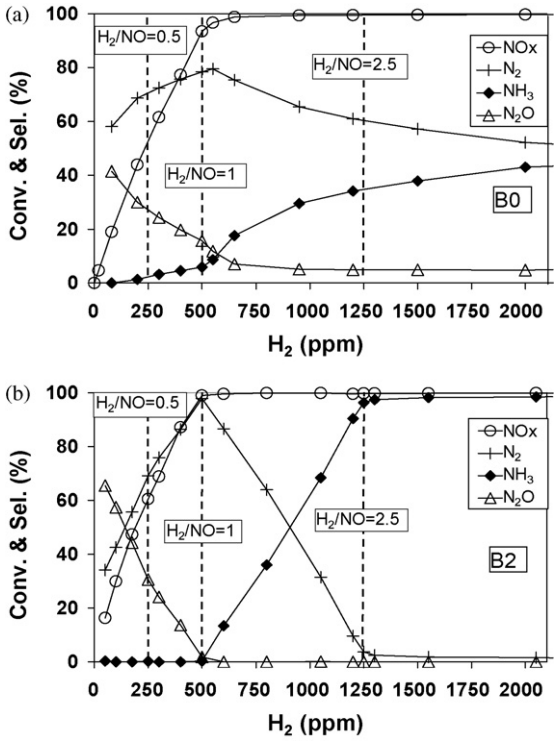

Fig. 1. NO_x conversion and N_2, NH_3, and N_2O selectivities during steady-state NO reduction by H_2 at 360 °C (a) BaO/Al_2O_3 (B0); (b) $Pt/BaO/Al_2O_3$ (B2); (500 ppm NO and varied H_2 concentration).

In these experiments the feed NO concentration was fixed at 500 ppm while the feed H_2 concentration was varied over a wide range (0–2000 ppm). The feed flow rate corresponded to a GHSV of about 60,000 h^{-1}. The overall N_2O, N_2 and NH_3 selectivity trends with respect to increasing H_2 concentration are qualitatively similar for the two catalysts with some differences in the rate of change of selectivities. All three catalysts exhibited a maximum in the N_2 selectivity at H_2/NO of about unity, which is the stoichiometry for N_2 production from H_2 and NO.

The Pt and Pt/BaO catalysts exhibited nearly identical results over the entire range of feed H_2 concentration. A minor difference concerns the N_2 and NH_3 selectivities for H_2/NO > 2.5. The N_2 selectivity for the Pt catalyst (A3) was essentially immeasurable (0%) [34], whereas the Pt/BaO catalyst (B2) sustained a non-zero value (Fig. 1b). Similar differences were observed for the NH_3 selectivity. In the absence of H_2 in the feed, a measurable NO_x conversion was not observed under steady-state conditions; i.e. negligible NO decomposition. N_2O was the dominant product and N_2 the byproduct at low H_2 concentration. The N_2O selectivity decreased from its maximum value to a negligible level when the feed H_2/NO ratio approached unity. In this range of H_2 concentrations the corresponding N_2 selectivity increased to its maximum value; the sum of the N_2 and N_2O fractional selectivities summed to unity as little NH_3 was produced for H_2/NO < 1. At higher H_2 feed concentrations the N_2 selectivity decreased at the expense of an increase in the NH_3 selectivity; i.e. the N_2 selectivity approached 0% and the NH_3 selectivity approached 100% for the Pt and Pt/BaO catalysts. The formation of N_2O was negligible for both catalysts in this range of H_2 feed concentrations.

The behavior of the BaO catalyst resembled the Pt and Pt/BaO catalysts but the changes and extremes in the product selectivities were not as pronounced (Fig. 1a). A measurable activity for the BaO/Al_2O_3 catalyst was only achieved after the catalyst was exposed to elevated temperatures for a prolonged time. The activation temperature and duration of activation determined the activity of the BaO sample (e.g. higher temperatures required less time to completely activate). Specifically, the BaO catalyst was more selective to N_2 for H_2/NO < 0.5 but less selective to N_2 as H_2/NO approached unity. Moreover, the drop-off in the N_2 selectivity was not as sharp for H_2/NO > 1, maintaining a high N_2 selectivity (>50%) at 2000 ppm H_2. This is consistent with the measurable production of N_2 on the Pt/BaO catalyst for H_2/NO > 2.5; i.e. on the Pt catalyst the N_2 selectivity was essentially zero [34]. Since BaO has a much lower activity than Pt, as we show next in the context of Figs. 2 and 3, the contribution of BaO to the Pt/BaO activity is small but measurable.

Figs. 2 and 3 show the effect of Pt loading and space velocity on NO_x conversion and selectivity at 100 °C and 300 °C, respectively, for a feed having a H_2/NO ratio of 2.5. As expected, the NO_x conversion decreases with increasing GHSV for all cases. As seen in Fig. 2, at 100 °C, the Pt-free BaO catalyst (B0) had negligible activity while the catalyst with the lowest non-zero Pt loading (B1) had a much lower activity than

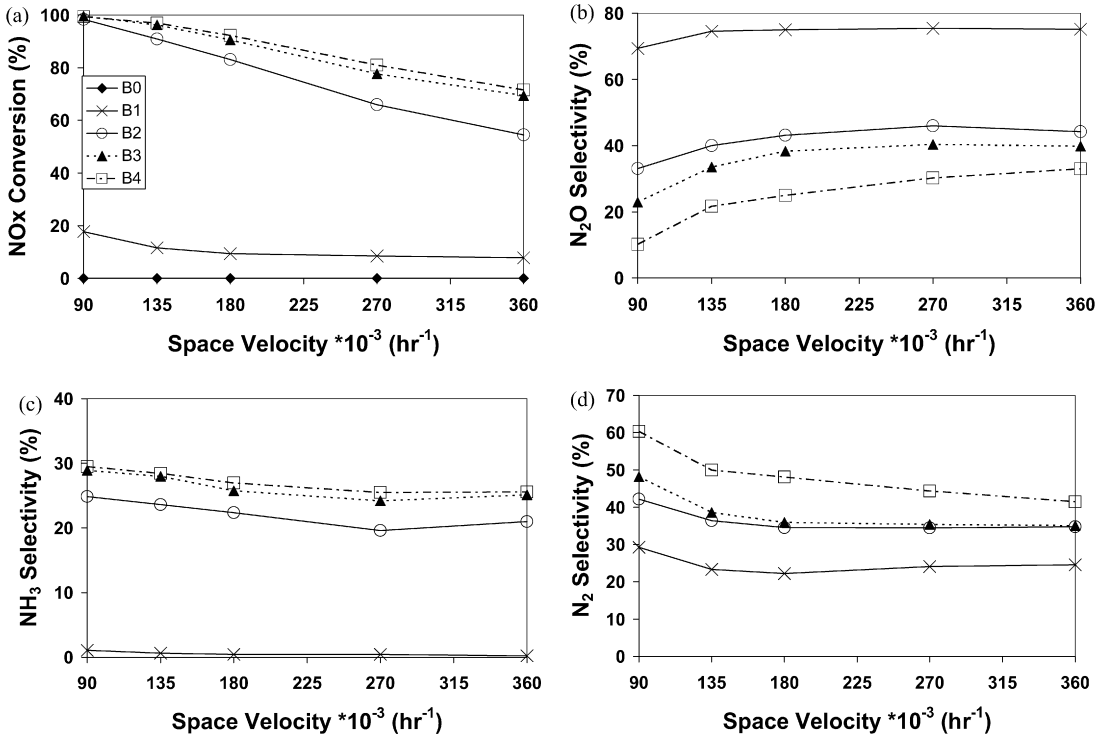

Fig. 2. Steady-state NO reduction by H_2 at 100 °C as a function of space velocity and Pt loading (a) NO_x conversion; (b) N_2O selectivity; (c) NH_3 selectivity; (d) N_2 selectivity (500 ppm NO and 1250 ppm H_2).

the catalysts with higher Pt loading. Catalysts B2, B3, and B4 exhibited similar trends with the activity increasing with increasing Pt loading (B2 to B4). The two catalysts with the highest loading (B3, B4) had negligible difference in the NO_x conversion. In general, the N_2O selectivity was highest at the lower conversions (higher GHSV), while the N_2 selectivity showed the opposite trend. The NH_3 selectivity ranged between 20 and 30% for the Pt-containing catalysts at 100 °C with only a

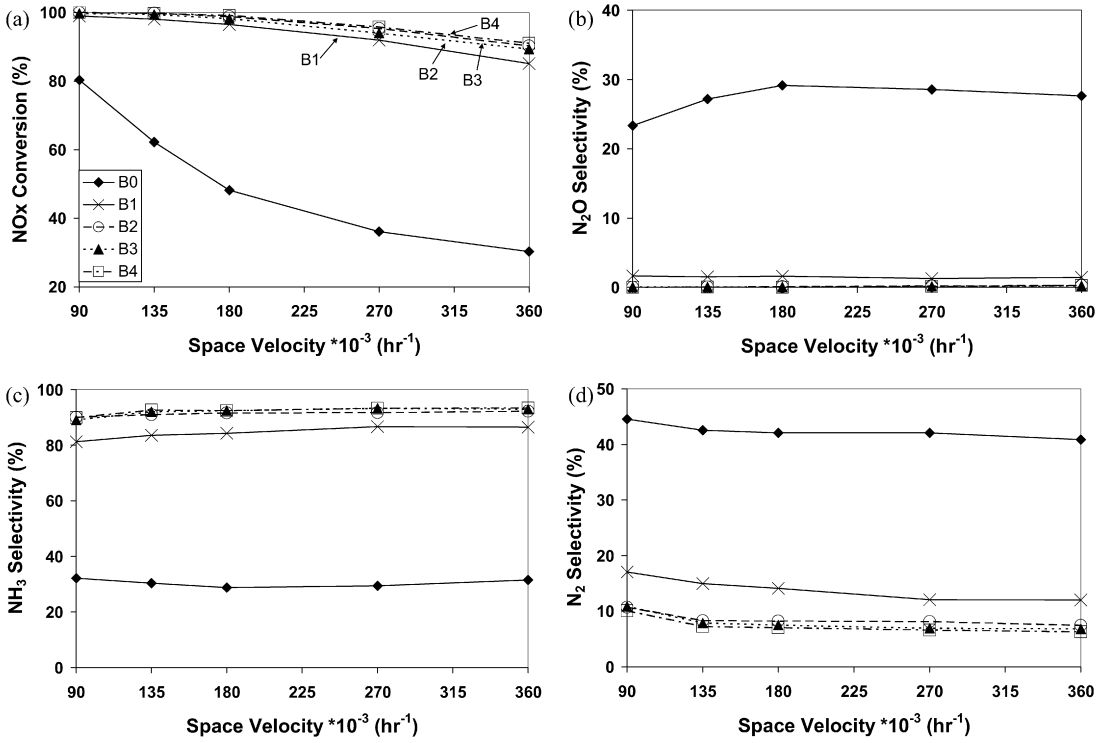

Fig. 3. Steady-state NO reduction by H_2 at 300 °C as a function of space velocity and Pt loading (a) NO_x conversion; (b) N_2O selectivity; (c) NH_3 selectivity; (d) N_2 selectivity (500 ppm NO and 1250 ppm H_2).

mild dependence on space velocity. At the same feed composition (H_2/NO = 2.5) but higher temperature (300 °C) the ammonia selectivity exceeded 85% for the same catalysts (Fig. 3). All of the catalysts containing Pt exhibited similar behavior in terms of NO_x conversion and product selectivities. Even catalyst B1, which contained only 0.32% Pt, achieved a similar NO_x conversion at this higher temperature and range of space velocities.

The dependence of NO_x conversion and product selectivities on the monolith temperature and Pt loading is shown in Fig. 4 for an anaerobic NO/H_2 feed. The light-off temperature increased with decreasing Pt loading showing the sensitivity to the Pt loading at low temperatures (The light-off point is defined as the temperature at which conversion increases rapidly and shows an inflection point). The selectivity trends for all three catalysts are similar. In general, the N_2O selectivity decreased with increasing temperature while the NH_3 and N_2 selectivities exhibited maximum values at intermediate temperature (Fig. 4c and d). The one exception is the lack of a N_2 selectivity maximum for the barium-only (B0) catalyst (Fig. 4d). The ammonia selectivity increased with temperature for a fixed feed composition and space velocity below 400 °C, as shown for the B3 catalyst in our previous study [34] and for the B0, B1, and B3 catalysts shown in Fig. 4. The NH_3 selectivity increased while the N_2 selectivity decreased with increasing Pt loading over the temperature range studied. The temperature at which the NH_3 selectivity maximum occurred was insensitive to the Pt loading, which corresponded to 400 °C for the three samples studied. On the other hand, the N_2 selectivity maximum moved to higher temperature with an increase in the Pt loading. Interestingly, for the B1 and B3 catalysts the N_2 selectivity had both a relative maximum and minimum as the temperature spanned the entire range.

Further experiments were carried out (not shown here) to confirm that the BaO catalyst (B0) was active. A blank experiment (no catalyst) was run in order to rule out contamination of the reactor system. Also, BaO/γ-Al_2O_3 powder and γ-Al_2O_3 powder were compared. Neither powder was initially active when exposed to 500 ppm NO and 1250 ppm H_2 (balance N_2) at 300 °C. Both samples were then heated to 600 °C in argon for 1 h and then the experiment was repeated at 300 °C. The BaO/γ-Al_2O_3 catalyst exhibited a 20% conversion while the γ-Al_2O_3 catalyst remained inactive. These experiments confirmed that BaO was indeed the active component but required the high temperature activation. Additional surface analysis was done in order to determine the active form of barium during NO reduction by H_2. Both fresh and activated samples of BaO were analyzed by X-ray photo-electron spectroscopy (XPS). The fresh sample was predominantly in the form of barium carbonate ($BaCO_3$) while the activated sample contained both BaO and $Ba(OH)_2$. No nitrogen was detected during the analysis for both the fresh and activated samples.

The dependence of the light-off temperature on NO concentration for a fixed concentration of H_2 (0.5%) on Pt/BaO is shown in Fig. 5. As the concentration of NO decreased the light-off temperature of NO reduction by H_2 also decreased, suggesting that the rate is negative order with respect to NO. Fig. 5b–d show that the dominant reaction prior to light-off is the formation of N_2O. At high NO_x conversion, the yield of N_2O decreased with increasing temperature at the expense of N_2 and NH_3 formation.

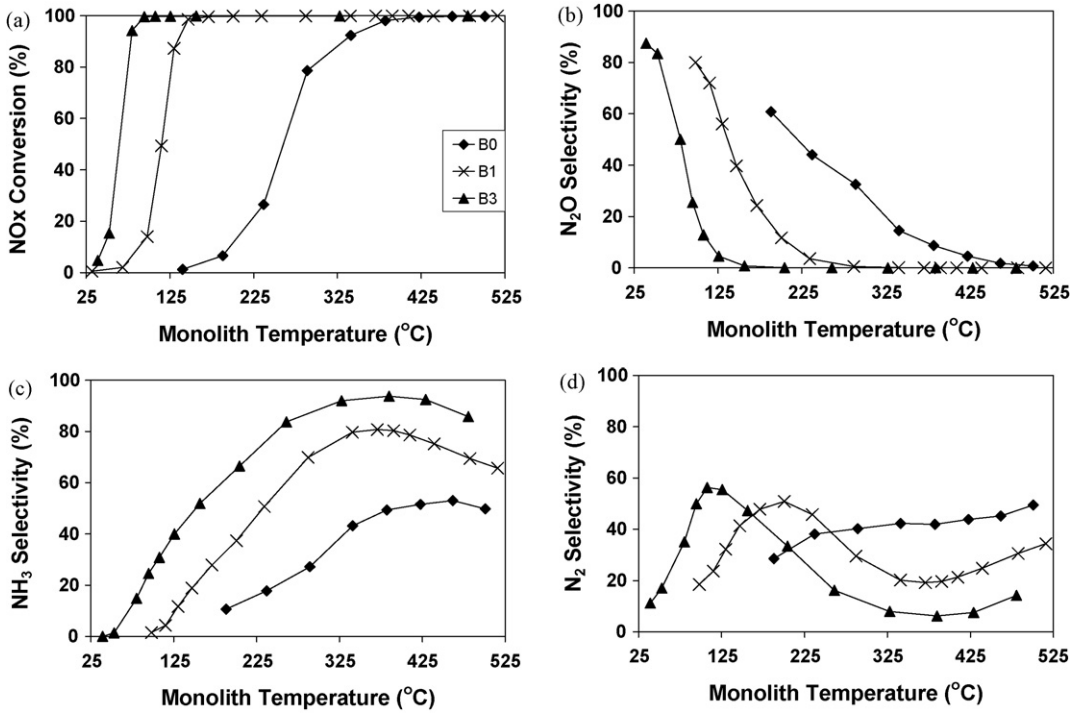

Fig. 4. Steady-state NO reduction by H_2 as a function of monolith temperature for catalyst B0, B1, and B3 (a) NO_x conversion; (b) N_2O selectivity; (c) NH_3 selectivity; (d) N_2 selectivity (500 ppm NO and 1250 ppm H_2).

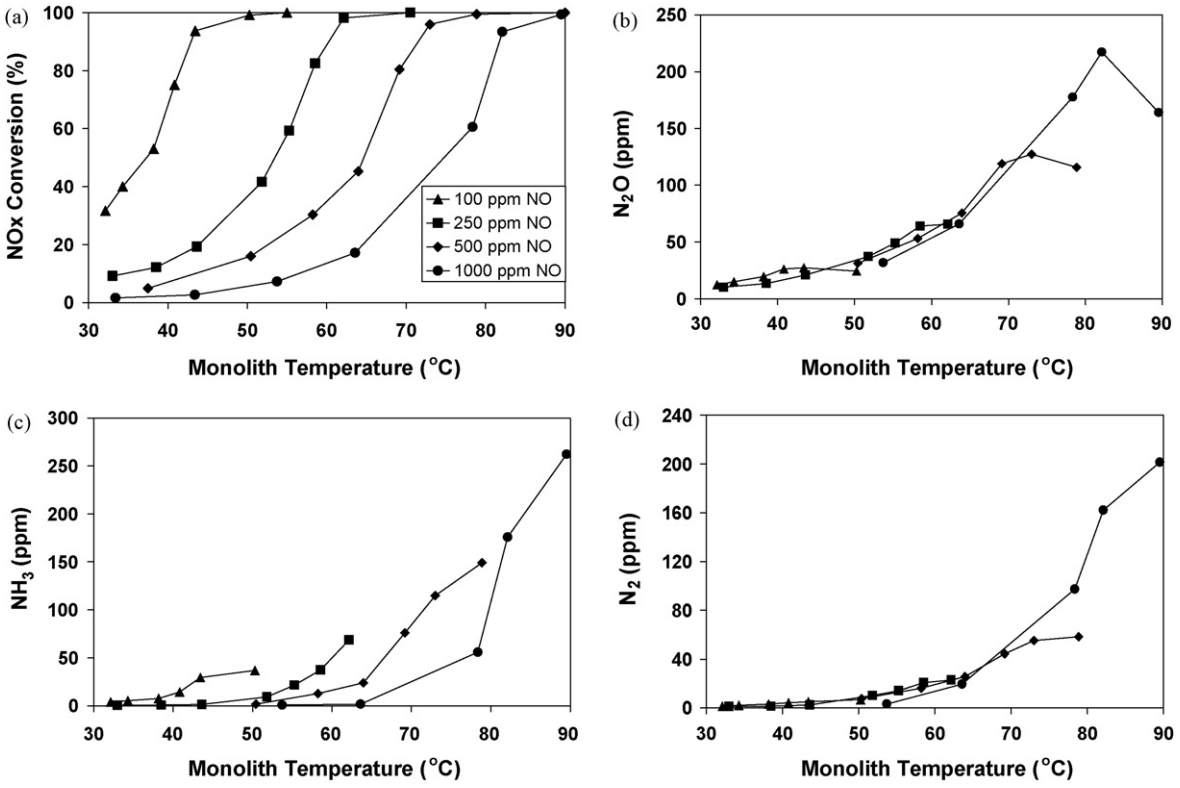

Fig. 5. Steady-state light-off curves for NO reduction by H_2 as a function of NO feed concentration for catalyst B2 (a) NO_x conversion; (b) N_2O selectivity; (c) NH_3 selectivity; (d) N_2 selectivity; (0.5% H_2 and varied NO concentration).

3.2. Aerobic NO_x reduction

The performance of the $Pt/Ba/Al_2O_3$, Pt/Al_2O_3, and BaO/Al_2O_3 catalysts were studied under steady-state conditions over a range of different feeds containing O_2. Fig. 6a–d show the NO_x conversion and product selectivities as a function of monolith temperature for several different H_2 concentrations. For these experiments, catalyst B3 was used with the space velocity, NO feed concentration and O_2 feed concentration fixed at 60,000 h^{-1}, 500 ppm, and 1%, respectively. It is convenient to define a stoichiometric number, S_N, which is the ratio of oxidizing to reducing components in the feed:

$$S_N = \frac{2[O_2] + [NO]}{[H_2] + 1.5[NH_3]} \quad (1)$$

The variation in the H_2 feed concentration for the current set of experiments spanned S_N values between 0.6 and 1.1.

An ''extinguished'' or ''quenched'' state is only reported for $S_N = 1.1$ because the time to reach steady-state for the quenched catalyst took up to one day (see below). In this state the NO_x conversion was very sensitive to small changes in the monolith temperature and the primary product was N_2O (Fig. 6b). Ignition occurred at about 50 °C, which was accompanied by a large increase in the NO_x conversion and monolith temperature. The adiabatic temperature rise was calculated to be 150 °C for 1.8% H_2 ($S_N = 1.1$) and measured at 130 °C. The difference in the measured and calculated values was attributed to heat losses in the reactor which are negligible under anaerobic conditions.

In the ignited state, the NO_x conversion exhibited a maximum at about 200 °C for the lean feed ($S_N = 1.1$) while the NO_x conversion remained at 100% for all of the rich and stoichiometric feeds. While N_2O was the main product in the extinguished state for the lean feed, N_2 and NH_3 were the main products in the ignited state for all the feeds. The N_2 selectivity generally increased with temperature in the ignited state while the NH_3 selectivity decreased. The NH_3 selectivity exhibited a strong sensitivity to the feed composition for S_N in the range of 1.10–0.95. For S_N less than 0.95, the NH_3 selectivity achieved 100% at approximately 250 °C and remained at that level up to 550 °C.

The experiments revealed evidence for steady-state multiplicity, manifested as a multi-valued dependence of the NO_x conversion on the feed temperature for the lean feed ($S_N = 1.1$). (As in previous plots, the data reported in Fig. 6 have the monolith temperature as the independent variable so the multiplicity is not evident in this form.) Upon ignition, a large increase in the monolith temperature (from 50 to 180 °C) and a small increase in the feed temperature ($\Delta T \sim 10$ °C) occurred simultaneously. The increase in feed temperature is presumably due to back radiation or conduction through the reactor wall.

It is interesting to note that the Pt/BaO catalyst required an inordinately long time to reach steady-state (up to 25 h), starting from the extinguished state with the $S_N = 1$ feed. An example result is shown in Fig. 7a. In this experiment, steady-state was achieved only after about 14 h for the extinguished catalyst. The NO_x effluent concentration increased slowly from

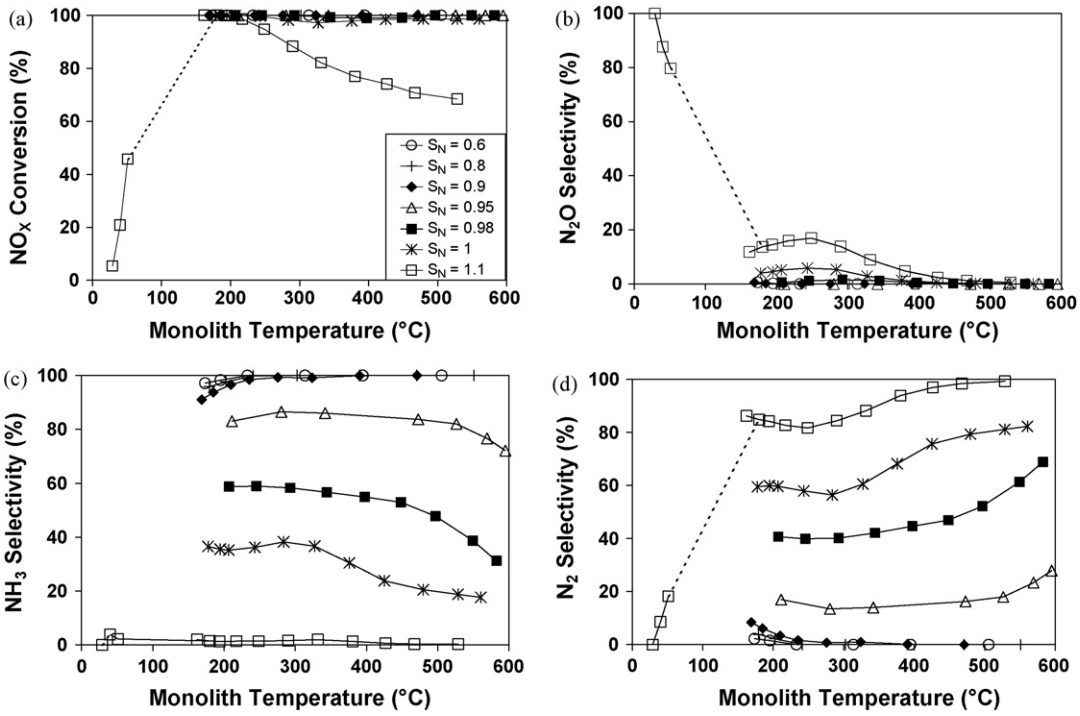

Fig. 6. Aerobic steady-state NO reduction by H_2 as a function of monolith temperature for catalyst B3 (a) NO_x conversion; (b) N_2O selectivity; (c) NH_3 selectivity; (d) N_2 selectivity (1% O_2, 500 ppm NO and varied H_2 concentration).

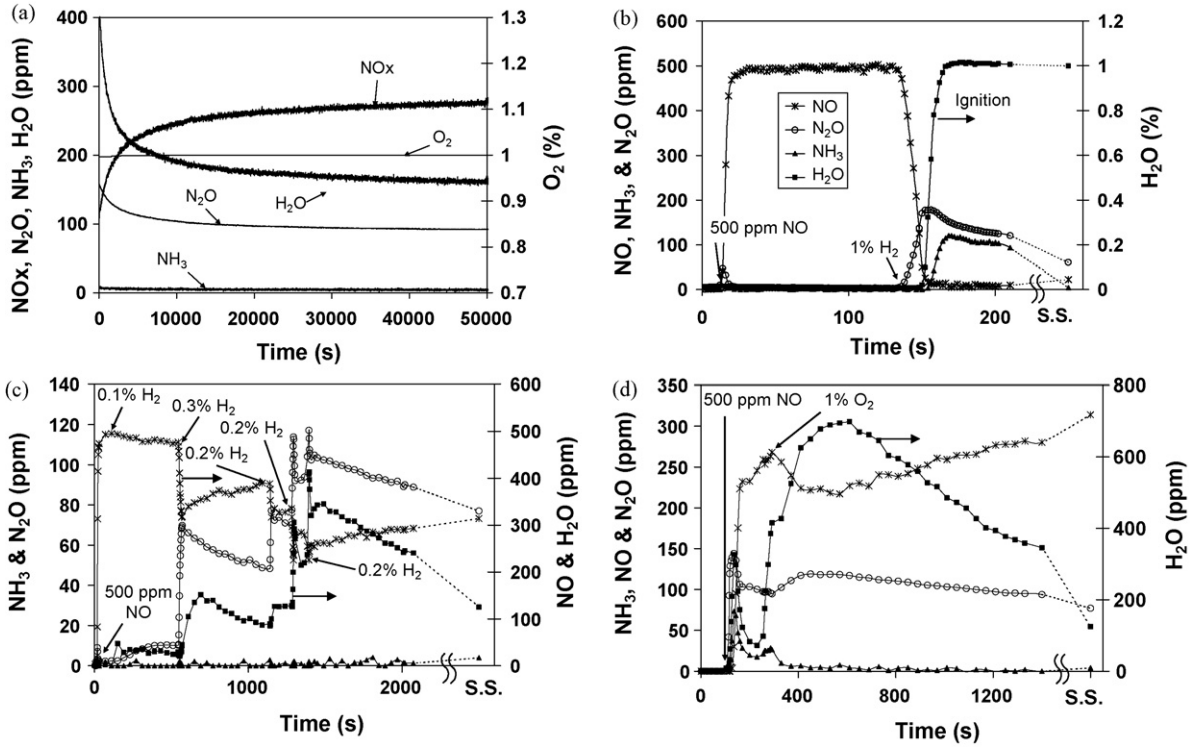

Fig. 7. Transient effluent concentration profiles for NO reduction by H_2 on catalyst B3 in the extinguished state at 45 °C (a) concentrations slowly approaching steady-state, $S_N = 1$; (b) order of addition of reactants to the reactor, $O_2 \rightarrow NO \rightarrow H_2$, $S_N = 2$; (c) order of addition of reactants to the reactor, $O_2 \rightarrow NO \rightarrow H_2$, slowly adding H_2 in increments, $S_N = 2$; (d) order of addition of reactants to the reactor, $H_2 \rightarrow NO \rightarrow O_2$, $S_N = 2$ (1% O_2, 500 ppm NO and 2.05% or 1.03% H_2).

100 ppm (this corresponds to 80% NO_x conversion) to a steady-state value of about 280 ppm (44% conversion). The main N-containing product was N_2O (i.e. 220 ppm NO was converted to 100 ppm N_2O, with the remainder to N_2). The measured effluent water concentration of 160 ppm was consistent with this N-containing product distribution.

The rate and order of reactant addition helped to determine the surface coverage of the Pt/BaO catalyst. Several experi-

ments were carried out in which the reactant order was fixed but the feed rate of the H_2 was varied. Ignition only occurred when H_2 was added abruptly. To illustrate, Fig. 7b shows the results of an experiment in which the catalyst was first exposed to a flowing feed of N_2 (99%) and O_2 (1%). At the 8 s point NO was admitted at the 500 ppm concentration level. After 130 s, the entire 1% H_2 was admitted. Ignition occurred approximately 25 s later. In contrast, in the experiment shown in Fig. 7c the same order of reactant addition was followed. The only difference was that H_2 was added more gradually. At the 130 s point, H_2 was fed at a rate giving a feed concentration of 1000 ppm (0.1%). At that point NO began to react, forming N_2O. Similar incremental increases in the H_2 concentration (as indicated in the figure) were then followed. After each H_2 addition more NO reacted to form a mixture of N_2O, H_2O, and N_2. However, ignition did not occur. Similar results were obtained when changing the order of reactants to $NO/O_2/H_2$, again with the addition of H_2 added gradually. In another set of experiment shown in Fig. 7d the reactant order was changed to $H_2/NO/O_2$. In this case the abrupt addition of O_2 after the catalyst had stabilized did not lead to ignition.

In order to elucidate the kinetic behavior of the lean feed at low temperature (<80 °C) a series of low conversion experiments were carried out to determine reaction orders. The reaction order with respect to H_2 surface concentration was measured by fixing the NO feed concentration while varying the H_2 feed concentration. Similarly, the reaction order with respect to NO surface concentration was measured by fixing the H_2 feed concentration while varying the NO feed concentration. For these experiments the reactor was run differentially (limiting reactant conversion <15%). The importance of diffusional limitations within the washcoat was determined by the Weisz-Prater criterion which states that pore diffusional limitations are negligible when the following inequality is true [35].

$$\frac{r_{\text{app}}\delta_{\text{w}}^2}{D_{\text{eff}}C_{\text{s}}} \ll 1 \tag{2}$$

where r_{app} is the apparent reaction rate (mol/cm^3/s), C_{s} is the concentration at the surface (mol/cm^3), δ_{w} is the washcoat thickness (cm), and D_{eff} is the effective pore diffusion of NO (cm^2/s). The effective pore diffusion of NO was estimated by

$$D_{\text{eff}} = D\frac{\varepsilon}{\tau} \tag{3}$$

where D is the limiting reactant diffusivity in Ar (cm^2/s), τ is the tortuosity factor, and ε is the porosity of the washcoat. The value of the Weisz-Prater modulus calculated from our experimental conditions is 0.00518, indicating that washcoat diffusional limitations were negligible. The limiting reactant surface concentration (concentration at the external surface of the washcoat) was estimated by the species balance

$$\dot{V}(C_{\text{in}} - C_{\text{out}}) = k_{\text{c}}P_{\Omega}L(C_{\text{avg.}} - C_{\text{s}}) = V_{\text{w.c.}}r_{\text{N}_2\text{O}}(C_{\text{s}}) \tag{4}$$

where C is the concentration (mol/cm^3), k_{c} is the mass transfer coefficient (cm/s), P_{Ω} is the perimeter of the channel (cm), $\dot{V}$ is the volumetric flow rate through each channel (cm^3/s), and L is the length of the monolith (2 cm). The subscripts "in", "out", "avg.", and "s" refer to the inlet, outlet, arithmetic average, and surface. The mass transfer coefficient was estimated from

$$Sh = \frac{4R_{\Omega}k_{\text{c}}}{D} \tag{5.a}$$

where the Sherwood number is approximately 4 (for rounded square channels) for fully developed flow, R_{Ω} is the hydraulic radius (cm), and D is the diffusivity of the limiting reactant in Ar (cm^2/s). [Remark: Following our earlier study [34], we estimated fully developed flow to be attained in less than 3% of the catalyst length.] For the conditions studied here the length for the flow to fully develop is 0.0158 cm (0.8% of the total length). Taking $Sh = 4$ and rearranging Eq. (5.a) gives

$$k_{\text{c}} = \frac{D}{R_{\Omega}} \tag{5.b}$$

Neglecting any diffusional limitations within the washcoat, the reaction rate was then calculated by

$$r_{\text{N}_2\text{O}}(C_{\text{s}}) = \frac{F_{\text{in}}X_{\text{NO}}S_{\text{N}_2\text{O}}}{V_{\text{w.c.}}} \tag{6}$$

where F_{in} is the feed rate of NO (mol/s), X is the conversion of NO, $S_{\text{N}_2\text{O}}$ is the selectivity to N_2O, and $V_{\text{w.c.}}$ is the volume of the washcoat (cm^3). Fig. 8a and b are plots of the rate versus the limiting reactant H_2 and NO concentrations, respectively. For the case of H_2 as the limiting reactant,

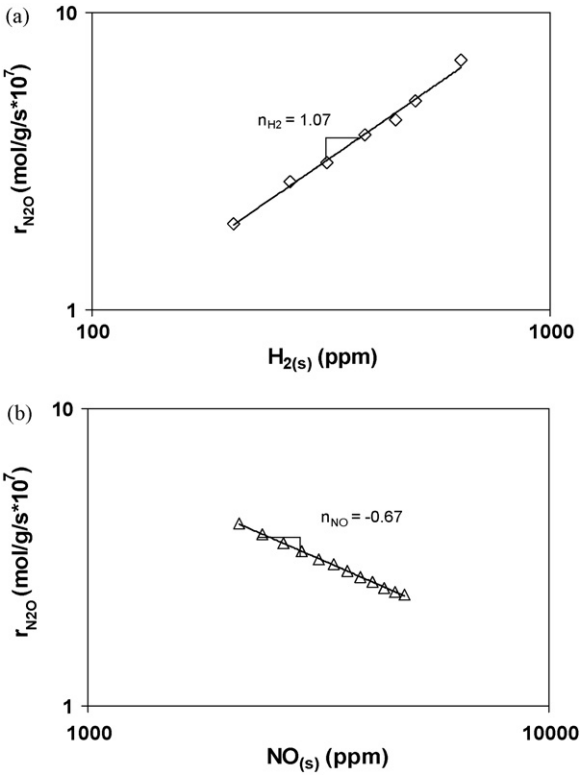

Fig. 8. Reaction rate vs. (a) H_2 surface concentration at 80 °C (200 ppm < H_2 < 700 ppm, 1000 ppm NO); (b) NO surface concentration at 53 °C (5500 ppm H_2, 2300 ppm < NO < 5000 ppm); catalyst B2.

the concentration of NO was set at 1000 ppm and the H_2 concentration was varied from 200 to 700 ppm at 80 °C, while for the case of NO as the limiting reactant, the NO concentration was varied from 2300 to 5000 ppm at 65 °C while fixing the H_2 concentration at 5500 ppm H_2. The experimental reaction orders of H_2 and NO were estimated to be 1.1 and −0.67, respectively. The negative order with respect to NO underscores the point that the rate of NO reduction is inhibited by NO, as evidenced by the ignition temperature dependence on NO feed concentration in Fig. 5.

As mentioned earlier, little differences were observed in the conversions and selectivities when comparing the Pt and Pt/BaO catalysts. The same was not true for the BaO catalyst. As seen in Fig. 9, which shows the dependence of conversion and selectivity on monolith temperature and S_N. While the qualitative trends in the conversion of H_2 and NO_x (Fig. 9a and b) are similar to those for the Pt (not shown) and Pt/BaO (Fig. 6), catalysts, the BaO catalyst has a more gradual, sigmoidal dependence on conversion rather than the abrupt dependence characteristic of the Pt-containing catalysts. Moreover, the BaO catalyst exhibits a high activity (H_2 conversion > 40%) at a much higher temperature (275 °C). Fig. 9c–e show the corresponding N_2, N_2O, and NH_3 selectivities. One notable difference from the Pt-containing catalysts is that NH_3 is produced under net oxidizing conditions on the BaO catalyst ($S_N > 1$) with a maximum corresponding to the maximum in NO conversion. For the $S_N = 0.8$ feed, the NH_3 selectivity increases monotonically with temperature.

Fig. 10 illustrates the dependence of NH_3 decomposition on the catalyst temperature (GHSV = 60,000 h^{-1}), H_2 concentration (GHSV = 60,000 h^{-1}, 520 °C), and the space velocity (520 °C). As expected, the conversion decreases with decreasing contact time on the Pt-based catalyst (Fig. 10a). The NH_3 conversion exceeds 30% at temperatures exceeding 510 °C at a

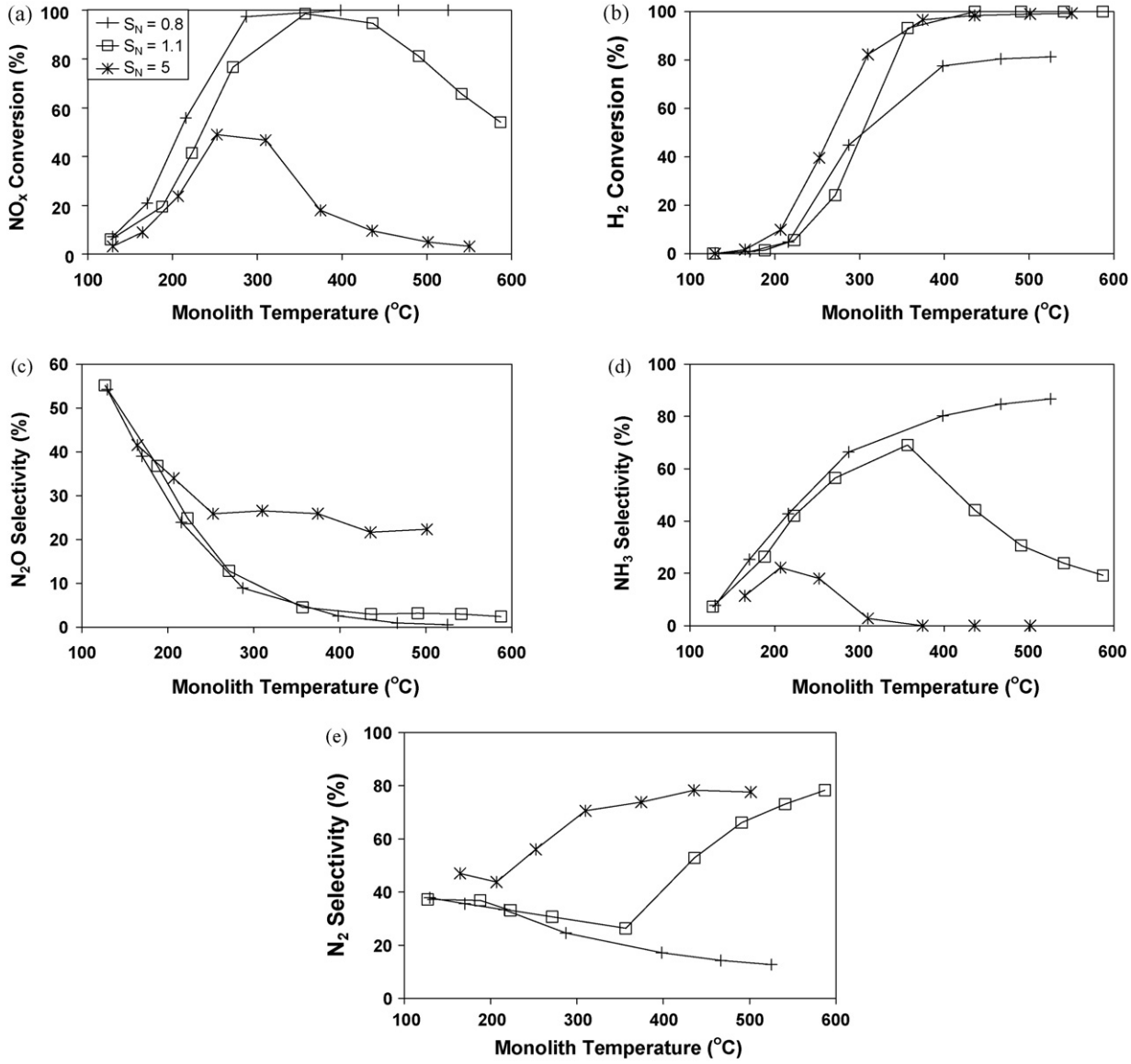

Fig. 9. Aerobic steady-state NO reduction by H_2 as a function of monolith temperature for catalyst B0 (a) NO_x conversion; (b) H_2 conversion; (c) N_2O selectivity; (d) NH_3 selectivity; (e) N_2 selectivity (1% O_2, 500 ppm NO and varied H_2 concentration).

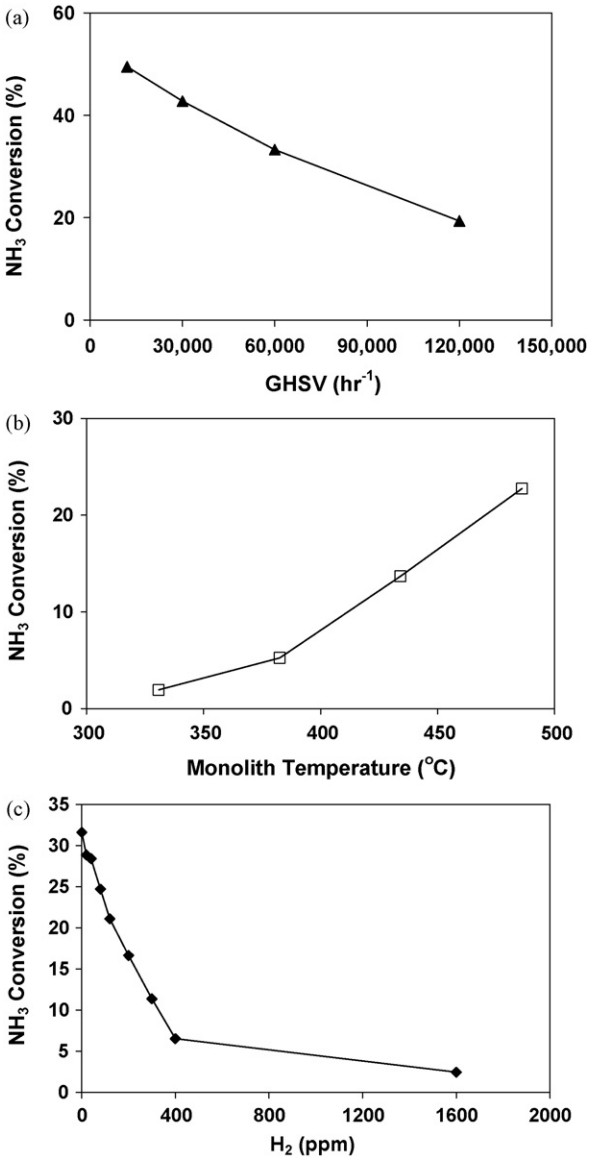

Fig. 10. NH_3 decomposition as a function of (a) flow rate at 520 °C, catalyst B4 (300 ppm NH_3); (b) monolith temperature, catalyst B2 (500 ppm NH_3); (c) H_2 concentration at 520 °C, catalyst B4 (500 ppm NH_3 and varied H_2 concentration).

space velocity of 60,000 h^{-1} (Fig. 10b). The decomposition is also inhibited by small amounts of H_2 (Fig. 10c).

The oxidation of NH_3 by O_2 is an important secondary reaction system due to the high selectivity to NH_3 from reaction between H_2 and NO. Fig. 11 shows typical light-off curves for ammonia oxidation as a function of monolith temperature at several different O_2 feed concentrations. In these experiments, different mixtures of O_2 (varied) and NH_3 (500 ppm) were fed over a $Pt/BaO/Al_2O_3$ catalyst (B3) while varying the temperature. The NH_3 oxidation system had a lights-off temperature of about 170–180 °C, forming a complex mixture of N_2O, N_2, NO, and NO_2. The NO selectivity increases monotonically with temperature while the selectivities of N_2O and NO_2 both exhibit maximum values at intermediate temperature. The maximum in N_2O selectivity is broad and occurs between 230 and 330 °C, whereas the NO_2 selectivity maximum occurs between 370 and 410 °C.

The dependencies of the selectivities of NO, NO_2, and N_2O on the oxygen concentration for a fixed monolith temperature of 390 °C are shown in Fig. 12. Between 500 and 2000 ppm of added O_2, the product distribution changes dramatically. At low concentrations of O_2 (<0.3%) the NO and N_2O selectivities initially increase (see Fig. 12b for detail). The N_2 (NO) selectivity decreases (increases) sharply with small increases in the O_2 concentration. The NO selectivity achieves a maximum value at ca. 0.3% O_2, beyond which it decreases gradually. This moderate decrease with increasing O_2 is accompanied by an increase in the NO_2 selectivity, indicating the onset of NO oxidation. In this higher O_2 concentration regime (>1%) the N_2O and N_2 selectivities remain nearly constant at about 12–14% and 16–18%, respectively.

Another important reaction system is the reduction of NO by NH_3. During the regeneration of a NO_x trap with H_2 the effluent may contain NH_3, which is formed by the reaction between H_2 and NO, and unreacted H_2. Fig. 13 shows the effect of feed H_2 concentration on the extent of the reaction between NO and NH_3 at a temperature of 285 °C for catalyst B3. The product (N_2, N_2O) selectivity here is based on the NO_x and NH_3 reacted. In the absence of feed H_2 the conversions of NH_3 and NO are 67.7% and 100%, respectively. An increase in the H_2 feed concentration to 500 ppm resulted in a sharp decrease in the NH_3 conversion to about 1%. Both the NO and H_2 conversions are essentially complete with N_2 being the only product. *This result clearly indicates that H_2 is a more effective reductant than NH_3 under these conditions.*

The NH_3–NO–H_2 system (500 ppm each) was further studied over the temperature range 20–500 °C as shown in Fig. 14a. In this set of experiments both N_2 and H_2 were measured directly with the mass spectrometer. Fig. 14a shows the measured effluent concentrations for all of the species. Fig. 14b shows the NO and NH_3 conversions and effluent concentration of N_2 and N_2O results with no H_2 in the feed. The H_2–NO reaction exhibited a light-off at about 90 °C. In the temperature range between 100 and 180 °C the effluent concentration of NH_3 exceeded the feed value due to the reduction of NO by H_2 (as indicated by the decrease in the NO and H_2 concentrations). The reaction between NO and H_2 produces a mixture of N_2O, NH_3, and N_2 that varies with temperature. N_2O is an important product at low temperatures, while NH_3 is only formed at intermediate temperatures and N_2 is the only product at high temperature. At temperatures exceeding 330 °C the effluent NH_3 concentration is below the feed value due to ammonia decomposition (as evidenced by the increase in the H_2 and N_2 concentrations). By comparison, in the absence of H_2 in the feed, the equimolar feed of NH_3 and NO reaction (500 ppm each) lights-off at a higher temperature (170 °C) on the same catalyst B2 (Fig. 14b). The reduction of NO by NH_3 is highly selective to N_2. After light-off, the conversion of NO_x is essentially complete while the ammonia conversion is about 66% until NH_3 begins to decompose above 330 °C. The production of N_2O is only important at lower temperatures.

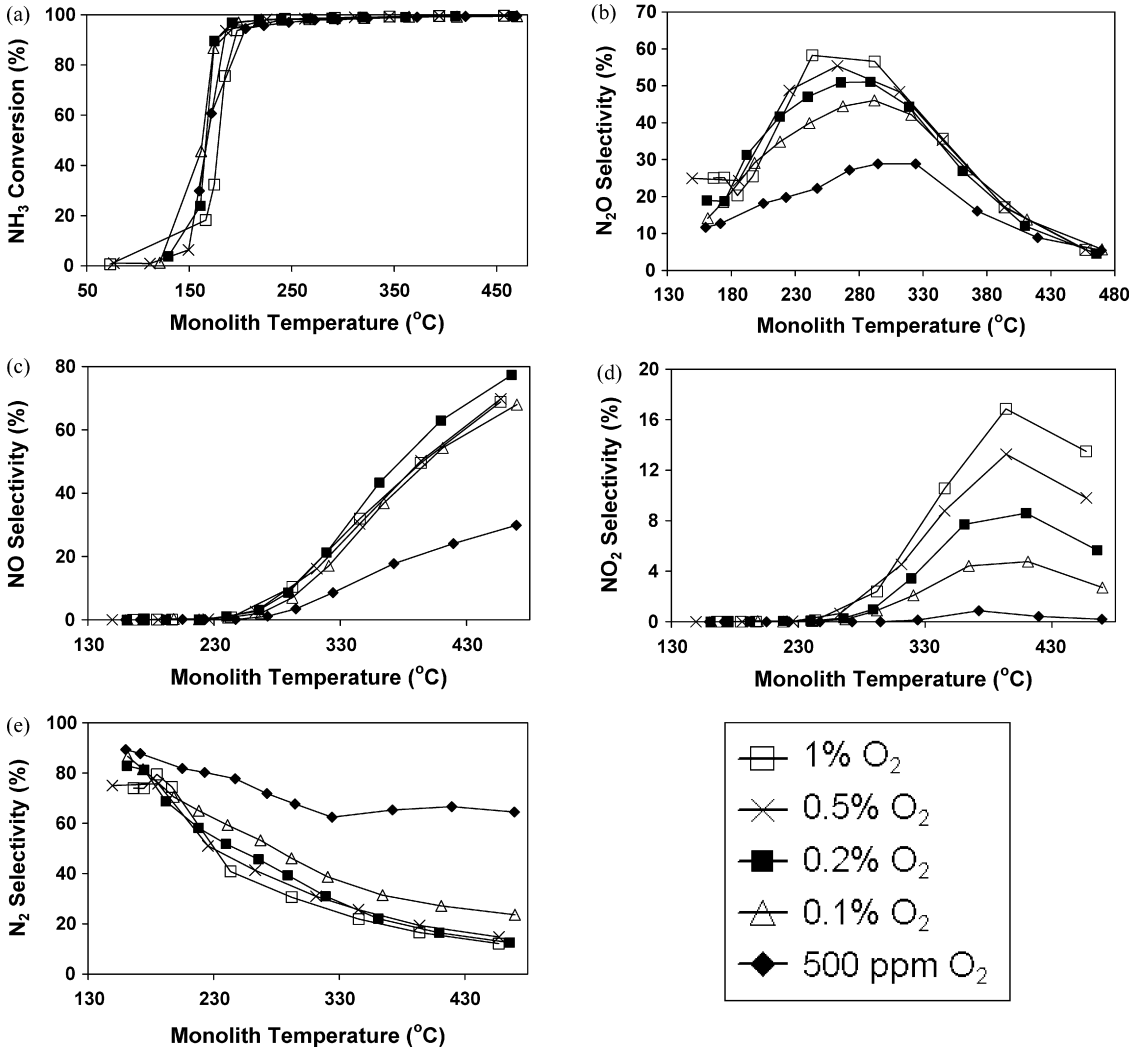

Fig. 11. Steady-state NH_3 oxidation as a function of monolith temperature for catalyst B3 (a) NH_3 conversion; (b) N_2O selectivity; (c) NO selectivity; (d) NO_2 selectivity; (e) N_2 selectivity (500 ppm NH_3 and varied O_2 concentration).

An experiment was performed with the same catalyst but containing only 500 ppm NH_3 in a balance of Argon. The ammonia (decomposition) conversion was compared to a feed containing 500 ppm each of NH_3, H_2, and NO (Fig. 14a). The intent was to quantify the extent of NO reduction by NH_3 in the presence of H_2. Fig. 15 shows that the difference in the NH_3 conversions for both cases is negligible, suggesting the NH_3 conversion that occurs in the presence of H_2 and NO is by decomposition only. Moreover, the H_2–NO reaction at high temperatures (>300 °C) does not affect the rate of NH_3 decomposition.

4. Analysis of experimental results and discussion

A comprehensive study has been carried out for several of the key reaction systems occurring during NO_x storage and reduction on model Pt/BaO, Pt, and BaO monolith catalysts. The effects of catalyst temperature, flow rate, and feed composition on steady-state conversion and product selectivities elucidate the reaction pathways and the contribution of the BaO storage component.

4.1. Rate controlling regimes and light-off

Most of the experimental results were obtained by varying the catalyst temperature over a wide range in order to span the low to high conversion states. Light-off was observed for many of the reaction systems. To the left of the light-off temperature the conversion is low and the rate is limited by chemical rate processes. To the right of the light-off temperature the conversion of the limiting reactant nears completion and the rate is strongly influenced by mass transport effects, which may be transverse external and/or washcoat diffusion limitations. The dependence of the light-off temperature on the feed concentration of a reactant provides some information about whether that species inhibits or enhances the rate. In general, the rate is positive (negative) order with respect to the limiting reactant if the light-off temperature decreases (increases) with an increase in the limiting reactant concentration [36]. The data shown in Fig. 5 clearly reveals that NO inhibits NO reduction. Captain et al. [37] observed the inhibition of NO on propylene light-off temperature on a Pt/Al_2O_3 catalyst. Specifically, when 900 ppm of NO was added to a feed stream containing 900 ppm

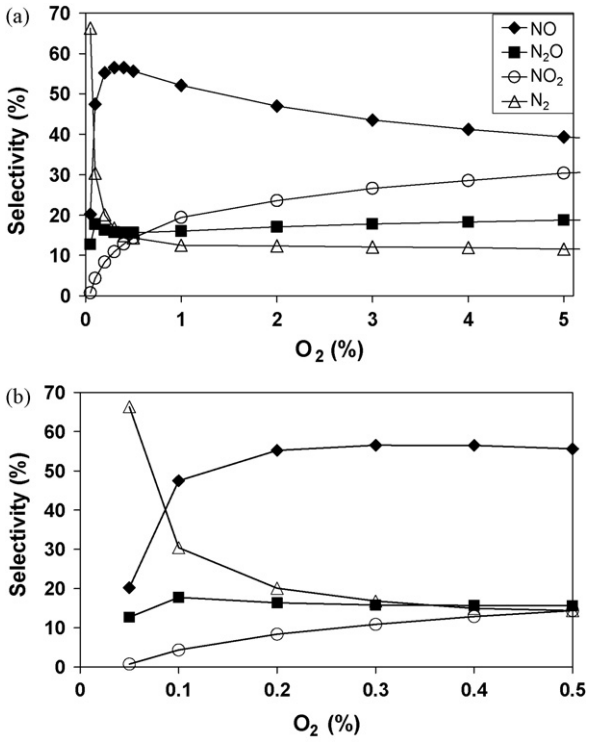

Fig. 12. Product selectivities from NH_3 oxidation on catalyst B3 as a function of O_2 concentration at 390 °C (a) 0–5% O_2; (b) 0–0.5% O_2 (500 ppm NH_3 and varied O_2 concentration).

C_3H_6 and 1% O_2, the light-off temperature increased by 50–70 °C. Variations in the selectivities reflect differences in the relative rates of supply of reactants to the catalyst.

In order to explore the issue of rate control in more detail, an estimate of the two key mass transfer characteristic times is revealing. The transverse Peclet number is the ratio of the characteristic transverse (radial) diffusion time to characteristic flow or convection time; i.e. $P = t_d/t_c = (R_\Omega^2/D_i)/(L/u_f)$, where L is the length of the monolith channel, u_f is the average gas velocity in the channel, R_Ω is the hydraulic radius defined as the ratio of the channel area (A_Ω) to channel perimeter (P_Ω), and D_i is the gas phase diffusion coefficient of the limiting reactant i. A value of P that is much greater than unity implies significant

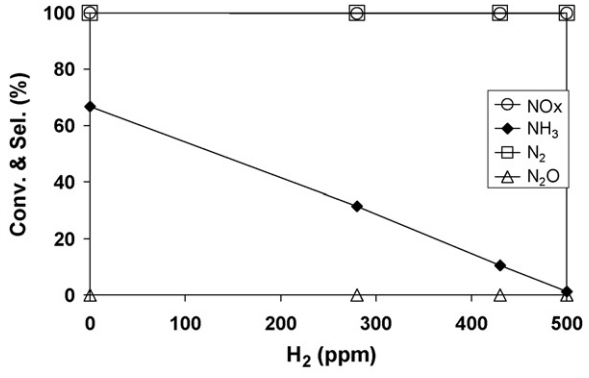

Fig. 13. NH_3 and NO conversion and N_2 and N_2O selectivities on catalyst B3 as a function of H_2 concentration at 285 °C (500 ppm NO, 500 ppm NH_3, and varied H_2 concentration).

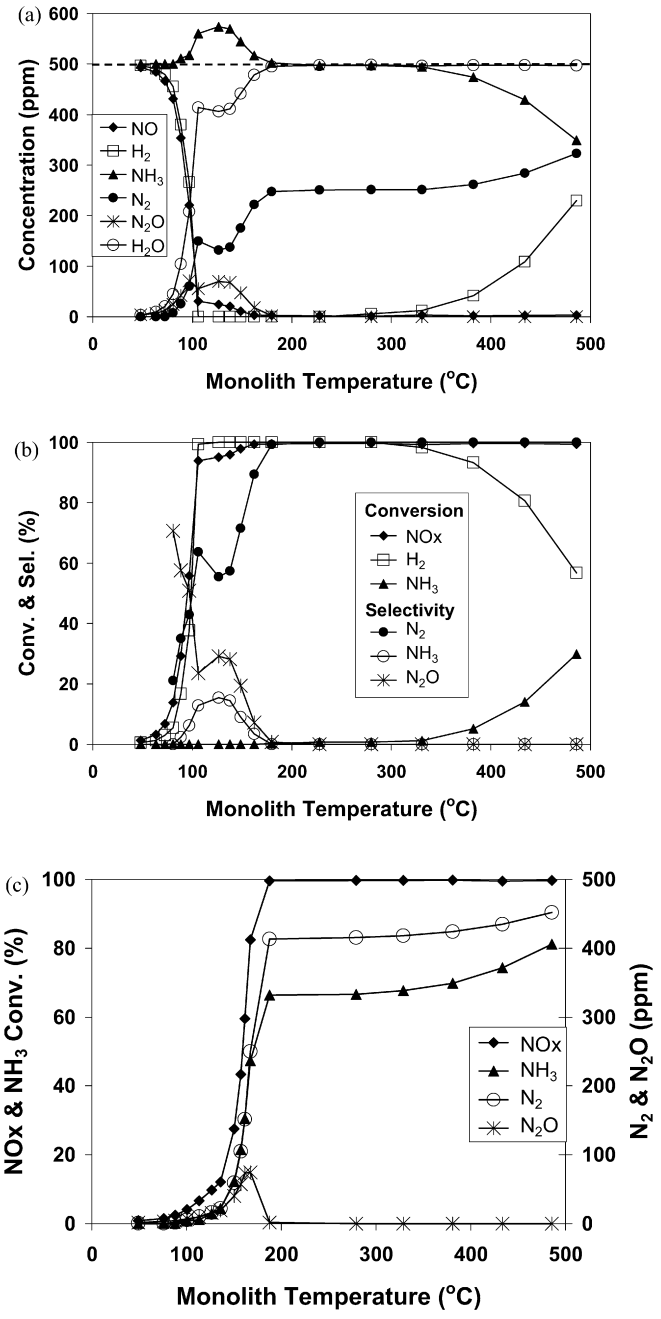

Fig. 14. NO reduction by H_2 and NH_3 as a function of temperature on catalyst B2 (a) effluent concentrations, 500 ppm H_2; (b) NO and NH_3 conversions and N_2 and N_2O effluent concentrations, 0 ppm H_2 (500 ppm NH_3, 500 ppm NO).

transverse (external) mass transfer/diffusion limitations, while a value much less than unity implies that the flow rate is the rate controlling process. Following our previous study [34], if we assume that NO is the limiting reactant and we provide estimates of the other parameters as follows; i.e. $L = 2$ cm; $u_f = 55$ cm/s (273 °C), $R_\Omega = 0.026$ cm; $D_i = 0.4$ cm^2/s, we estimate a transverse Peclet number $P = 0.046$. This indicates that the axial convection is slower than the transverse diffusion. Under these conditions the limiting reactant conversion will be nearly complete if there are no kinetic limitations and the product distribution will be determined primarily by the feed

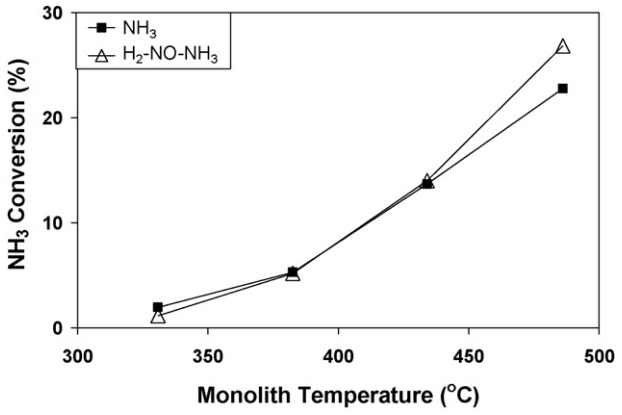

Fig. 15. NH_3 decomposition in the presence and absence of H_2 and NO as a function of temperature on catalyst B2; (500 ppm NH_3, 500 ppm NO, 500 ppm H_2).

composition and global reaction stoichiometries. The conventional axial Peclet number ($Pe_x = u_f L/D_i$) is the ratio of convection time to axial diffusion time. We estimate its value to be approximately 275, indicating that axial diffusion is unimportant relative to axial convection in the current system; i.e. plug flow behavior.

4.2. $NO + H_2 + O_2$ reaction system

In our previous study, we reported data and analysis for the anaerobic $NO + H_2$ on Pt/BaO catalyst [34]. Here, we summarize the main findings from that study to provide a framework for evaluating the aerobic reaction system ($NO + H_2 + O_2$ on Pt and Pt/BaO). The global reactions occurring in the anaerobic system are:

$$NO + 0.5H_2 \rightarrow 0.5N_2O + 0.5H_2O \quad (R1)$$

$$NO + H_2 \rightarrow 0.5N_2 + H_2O \quad (R2)$$

$$NO + 2.5H_2 \rightarrow NH_3 + H_2O \quad (R3)$$

At low temperatures (<150 °C) N_2O is the major product, with N_2 and NH_3 being the principal products at higher temperature. As we reported previously, H_2 reacts with NO below the light-off temperature, and as we discuss in more detail below, this occurs even in the presence of gas phase O_2. The selectivities to the N-containing products are largely determined by the feed ratio relative to the global reaction stoichiometries of (R1), (R2), and (R3). Note that the direct decomposition of NO produces O_2 which in the presence of hydrogen will react to form water:

$$NO \rightarrow 0.5O_2 + 0.5N_2 \quad (R4)$$

$$H_2 + 0.5O_2 \rightarrow H_2O \quad (R5)$$

We did not observe any NO conversion at steady-state below 360 °C. This is due to the self-poisoning caused by the blocking of platinum sites by oxygen from the dissociation of NO. Pirug and Bonzel [38] reported that the desorption of O_2 only occurs above 700 K on polycrystalline Pt catalyst. In the presence of H_2, NO is easily converted to N_2. A mechanistic interpretation is that as H_2 scavenges oxygen adatoms deposited by decomposing NO, freeing up sites for additional NO decomposition. Indeed it is noted that steady-state NO reduction to N_2 (R2) is the stoichiometric sum of reactions (R4) and (R5).

The low but non-zero steady-state conversion of NO obtained at temperatures below the light-off temperature reveals the interesting result that H_2 will react largely with NO, even in the presence of a large excess of O_2 (Fig. 6a). An analysis of the steady-state product distribution in Fig. 7a indicates that of the 230 ppm NO that react, 200 react to form 100 ppm of N_2O, while the remaining 30 ppm are reduced to N_2. The stoichiometries of the overall reactions (R1), (R3), and (R4) require the corresponding production of 130 ppm H_2O; the data indicate 150 ppm H_2O is produced. The difference is probably the result of reaction between H_2 and oxygen supplied from gas phase O_2 via reaction (R5). Taken together, these observations suggest that NO is effective in blocking the adsorption of gas phase O_2. The delicate nature of the startup procedure illustrated in Fig. 7 corroborates a mechanism in which a fraction of the NO adspecies reacts with the small amount of hydrogen that is able to adsorb or displace NO. This leads to N_2O formation. The gradual admission of H_2 enables a slow, isothermal reaction of a small amount of H_2 with adsorbed NO (Fig. 7c). On the other hand, an abrupt admission of H_2 causes a larger fraction of H_2 to adsorb and react with NO, causing local heating and the freeing of empty sites for dissociative O_2 adsorption and hydrogen oxidation, ultimately leading to light-off (Fig. 7b).

The following sequence of steps is proposed to explain these data, following our previous study [34]:

$$NO + Pt \leftrightarrow NO - Pt \quad (S1)$$

$$H_2 + 2Pt \leftrightarrow 2H - Pt \quad (S2)$$

$$NO - Pt + H - Pt \rightarrow N - Pt + OH - Pt \quad (S3)$$

$$NO - Pt + N - Pt \rightarrow N_2O + 2Pt \quad (S4)$$

$$H - Pt + OH - Pt \rightarrow H_2O + 2Pt \quad (S5)$$

$$2N - Pt \rightarrow N_2 + 2Pt \quad (S6)$$

This mechanism is consistent with a slow rate of NO bond scission at temperatures below 150 °C with an activation energy reported by Gruyters et al. [39] and Caballero and Vicente [40] to be 107.8 and 117.6 kJ/mol, respectively. At temperatures between 50 and 150 °C the N_2O selectivity decreases while the N_2 selectivity increases. This is a result of an increase in the rate of NO bond scission, making N_2 the preferred product. The high N_2O selectivity at low temperature is likely due to a predominantly covered surface by NO favoring reaction (S4). Once N_2O is formed, the NO covered surface prevents N_2O from readsorbing and reacting with H_2 (secondary reaction). Hecker and Bell [8] also observed a NO saturated surface when the NO_x conversion was less than 60%. The presence of a NO covered surface will also inhibit the dissociation of NO [41],

which favors N_2O formation. Siera et al. [42] proposed that N_2O may need adjacent vacant platinum sites in order to decompose and that the decrease in N_2O selectivity is due to the rate of NO desorption increasing [43] and NO decomposition increasing [41]. Transient TAP (temporal analysis of products) experiments carried out in our laboratory and which will be reported elsewhere suggest that adsorbed hydrogen abstracts O from adsorbed NO (step (S3)), enabling the adsorbed N to react with NO to form N_2O [44]. These results follow from the work of Hecker and Bell [8], who proposed that NO dissociation results from abstraction of O from adsorbed NO by adsorbed H (step (S3)). Gland and Kollin [45] proposed that hydrogen can displace adsorbed NO.

4.3. Kinetic analysis for anaerobic NO reduction by H_2

In order to explain the low temperature experimental results involving NO and H_2 in the absence of O_2 we propose here a simplified kinetic model for the reduction of NO by H_2 at low temperatures in which N_2O is the main product ($T < 50\ ^\circ C$; Figs. 5 and 8). Assuming pseudo-steady-state for the adsorbed species and mass action kinetics (except for H_2 adsorption which we assume to be first-order and irreversible) and neglecting the N_2 and NH_3 formation reactions, the following balances hold:

$$\text{NO}-\text{Pt}: \quad k_1 P_{NO}\theta_{Pt} - k_{-1}\theta_{NO} - k_4\theta_{NO}\theta_N - k_3\theta_{NO}\theta_H = 0 \tag{7}$$

$$\text{H}-\text{Pt}: \quad 2k_2 P_{H_2}\theta_{Pt} - k_3\theta_{NO}\theta_H - k_5\theta_{OH}\theta_H = 0 \tag{8}$$

$$\text{N}-\text{Pt}: \quad k_3\theta_{NO}\theta_H - k_4\theta_{NO}\theta_N = 0 \tag{9}$$

$$\text{OH}-\text{Pt}: \quad k_3\theta_{NO}\theta_H - k_5\theta_{OH}\theta_H = 0 \tag{10}$$

$$\text{Overall}: \theta_{OH} + \theta_{NO} + \theta_H + \theta_N + \theta_{Pt} = 1 \tag{11}$$

where k_i is the rate constant for step i and k_{-i} is the corresponding rate constant for the reverse of step i. The OH and N species balances, respectively, give:

$$\theta_N = \frac{k_3}{k_4}\theta_H \tag{12}$$

$$\theta_{OH} = \frac{k_3}{k_5}\theta_{NO} \tag{13}$$

The rates of production of N_2O and H_2O are given by

$$r_{N_2O} = r_{H_2O} = k_4\theta_{NO}\theta_N = k_3\theta_{NO}\theta_H = k_5\theta_{OH}\theta_H \tag{14}$$

The above equation may be solved to get explicit expressions for the various coverages and the reaction rate in terms of the rate constants and partial pressures (P_{NO} and P_{H_2}). We consider here the limiting case in which

$$\frac{2k_2 P_{H_2}}{k_1 P_{NO}} \ll 1, \tag{15}$$

is satisfied. This limiting case corresponds to H_2 adsorption being the rate limiting step on a mostly NO covered surface, encountered when there is sufficient NO relative to H_2 in the mixture. In this case, it can be shown that the following solution holds:

$$\theta_H = \left(\frac{2k_2 P_{H_2}}{k_1 P_{NO}}\right)\frac{k_1}{2k_3 K_{NO}}, \quad K_{NO} = \frac{k_1}{k_{-1}} \tag{16}$$

$$\frac{\theta_{NO}}{\theta_{Pt}} = K_{NO}P_{NO}, \quad \theta_N = \frac{k_2 P_{H_2}}{k_4 K_{NO} P_{NO}} \tag{17}$$

$$\theta_{OH} = \frac{k_3}{k_5}\theta_{NO} \tag{18}$$

$$r_{N_2O} = \frac{k_2 P_{H_2}[1 - (k_1(k_3 + k_4)/2k_3k_4K_{NO})]}{[1 + (1 + (k_3/k_5))K_{NO}P_{NO}]} \tag{19}$$

If we further make the assumption that $k_1/2k_4K_{NO} \ll 1$ (step 4 is much faster than the reverse of step 1), $k_1/2k_3K_{NO} \ll 1$ (step 3 is much faster than the reverse of step 1), and $k_3/k_5 \ll 1$ (step 5 is much faster than step 3), we get the result

$$r_{N_2O} = \frac{k_2 P_{H_2}}{1 + K_{NO}P_{NO}} \tag{20}$$

which simplifies further when $K_{NO}P_{NO} \gg 1$ to

$$r_{N_2O} = \frac{k_2 P_{H_2}}{K_{NO}P_{NO}} \tag{21}$$

The selected rate of N_2O versus surface H_2 and NO surface concentrations in Fig. 8 are consistent with the limiting kinetic rate expression (Eq. (20)). Since the order in NO is not -1 suggests that the catalyst surface is not completely covered by NO and therefore the full inhibition is not realized.

With the above assumptions, it is revealing to note that the result is analogous to the kinetics of CO oxidation on Pt, which has a rate that is first-order with respect to O_2 and negative first order in CO at sufficiently high CO concentration [46]. In fact, if one considers that the simplified $NO + H_2$ mechanism comprises steps (S1), (S2) and the following combined reaction step (which is the sum of (S3), (S4), and (S5)):

$$\text{NO}-\text{Pt} + \text{H}-\text{Pt} \xrightarrow{k_{4'}} 0.5N_2O + 0.5H_2O + 2\text{Pt} \tag{22}$$

It is easily shown that the rate is given by Eq. (21) if one further assumes that the coverage of H is negligible and the H_2 adsorption is first order with respect to H_2.

The data in Fig. 5 show that more complex kinetic behavior exists at temperatures exceeding 50 °C and higher P_{H_2}/P_{NO}. Both NH_3 and N_2 become more important products. As the temperature is increased the apparent orders with respect to NO for the three main products (N_2O, N_2, and NH_3) vary. For example, the N_2O formation is negative order with respect to NO at low temperatures and low P_{H_2}/P_{NO} and changes to zero then positive order at higher temperatures and higher P_{H_2}/P_{NO} values. For NH_3 formation the apparent order with respect to NO is negative order over a wider range of conditions. Regarding N_2O formation, at the higher P_{H_2}/P_{NO} ratios the kinetic regime clearly shifts to one in which the NO coverage is lower. Such a shift is similar to the above-mentioned CO oxidation in which there is a shift to a positive order dependence on CO at high O_2/CO. On the other hand, the negative-order that is apparent for NH_3 formation over a wide

range of conditions suggests that lower NO coverages are sufficient to inhibit the sequential addition of H to N to form NH_3. Clearly, a more detailed analysis is needed to explain these trends and is therefore the focus of a future study.

The NO_x conversion is observed to be complete above 200 °C under reducing conditions ($NO/H_2 < 1$; $S_N < 1$) and above 80% over a ca. 150 °C temperature window under oxidizing conditions (Fig. 6). Under reducing conditions NO is the limiting reactant with the major products being N_2 and NH_3. That NO is completely converted over the highly active Pt catalyst is not a surprise. On the other hand, nearly complete NO conversion is achieved for $S_N = 1.1$, albeit over a rather narrow temperature range. These findings are consistent with an earlier study by Burch and coworkers who reported that the maximum in lean NO_x conversion is an increasing function of the Pt loading [47].

4.4. Conversion in an isothermal monolith

The data show that the light-off temperature for the NO + H_2 reaction system is a sensitive function of the Pt loading and feed composition. Here, we use a simple monolith model to analyze key trends in the data. For the case of linear kinetics (first-order reaction), the conversion of the limiting reactant in an isothermal monolith is given by [48]

$$x = 1 - \alpha_1 \exp\left\{\frac{-\mu_1}{P(1 + (\mu_1/\Phi^2))}\right\} \tag{23}$$

Here α_1 and μ_1 are dependent on the shape of the flow area in the monolith channel (for the case of circular flow area, $\alpha_1 = 0.819$ and $\mu_1 = 0.914$ for $\Phi^2 \to \infty$ while $\alpha_1 = 1$ and $\mu_1 = 1.09$ for $\Phi^2 \to 0$). The parameters P and Φ^2 in Eq. (23) may be related to the various characteristics of the monolith channel by

$$P = \frac{R_\Omega^2 u_f}{L D_{mi}} \tag{24.a}$$

$$\Phi^2 = \frac{R_\Omega}{\delta_w}\frac{D_{ei}}{D_{mi}}\phi \tanh\phi \tag{24.b}$$

$$\phi = \delta_w \sqrt{\frac{k_v(T)}{D_{ei}}} \tag{24.c}$$

$$k_v(T) = k_{vo}\exp\left(\frac{-E}{RT}\right) = k_v(T_o)\exp\left[\frac{E}{RT_o}\left(\frac{T - T_o}{T}\right)\right] \tag{24.d}$$

$$\phi^2 = \phi_o^2 \exp\left[\gamma\left(\frac{T - T_o}{T}\right)\right], \quad \gamma = \frac{E}{RT_o}, \quad \phi_o^2 = \frac{\delta_w^2 k_v(T_o)}{D_{ei}} \tag{25}$$

Here δ_w is the effective washcoat thickness, D_{ei} (D_{mi}) is the diffusivity of the limiting reactant in the washcoat (gas phase) and $k_v(T)$ is the first-order rate constant based on unit volume of washcoat. [Note k_v is proportional to the precious metal dispersion times the metal loading.]

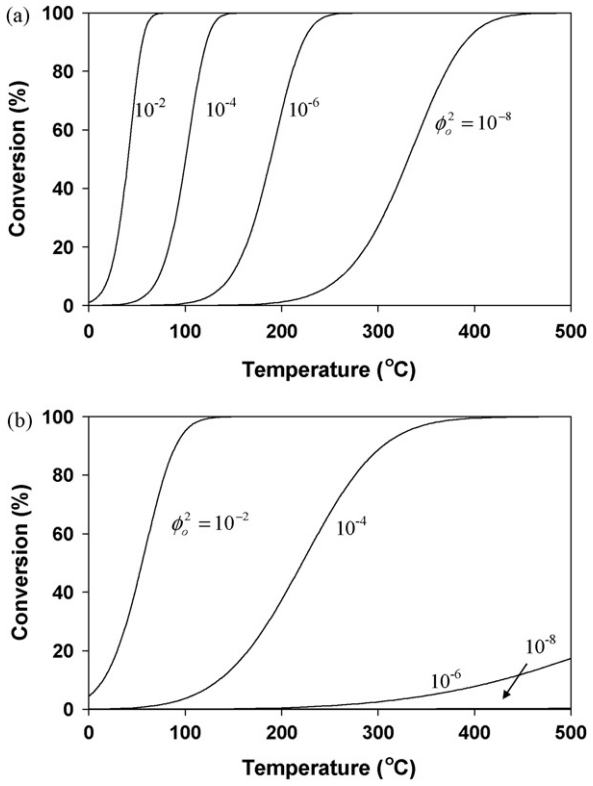

Fig. 16. Influence of precious metal loading on the light-off behavior of a monolith [for parameter values $P = 0.05$, $T_o = 27$ °C, $(R_\Omega/\delta_w)(D_{ei}/D_{mi}) = 1$] (a) $E/RT = 30$; (b) $E/RT_o = 15$.

Eq. (23) may be used to examine the general trends that show the influence of various design and operating variables on the light-off behavior of monoliths. The assumed parameter values ($P = 0.05$, $(R_\Omega/\delta_w)(D_{ei}/D_{mi}) = 1$) were estimated from experimental conditions and other information. For example, $P = 0.05$ corresponds to the 1 l/min flow rate giving a space velocity of 60,000 h^{-1}. Fig. 16a shows the influence of ϕ^2 on the conversion. ϕ^2 contains information about the washcoat activity (k_v) and diffusion (ϕ is Thiele modulus). As stated above, k_v is proportional to the exposed precious metal so Fig. 16 simulates the effect of loading on the light-off characteristics. We note that for a reaction with higher activation energy ($\gamma = 30$), decreasing the active site loading by a factor of 100 increases the light-off point by about 50 °C, and 300 °C for a decrease in loading by a factor of 10^6. We also note that the light-off occurs over a wider range of temperatures when the precious metal loading is reduced. Fig. 16b shows the same curve for a case of reduced activation energy ($\gamma = 15$). In this case, the light-off point moves by 150 °C to the right when the loading is decreased by a factor of 100. In addition, no light-off occurs within the temperature range shown ($T \leq 500$ °C) for the two lowest loadings. The effect of precious metal loading and P, which is proportional to the space velocity (GHSV), on conversion at 100 and 300 °C are plotted in Fig. 17. The predicted trends accurately represent the experimental results shown in Figs. 2a and 3a.

For the case of negative order kinetics, which as shown above is the case for NO in the NO + H_2 system at low

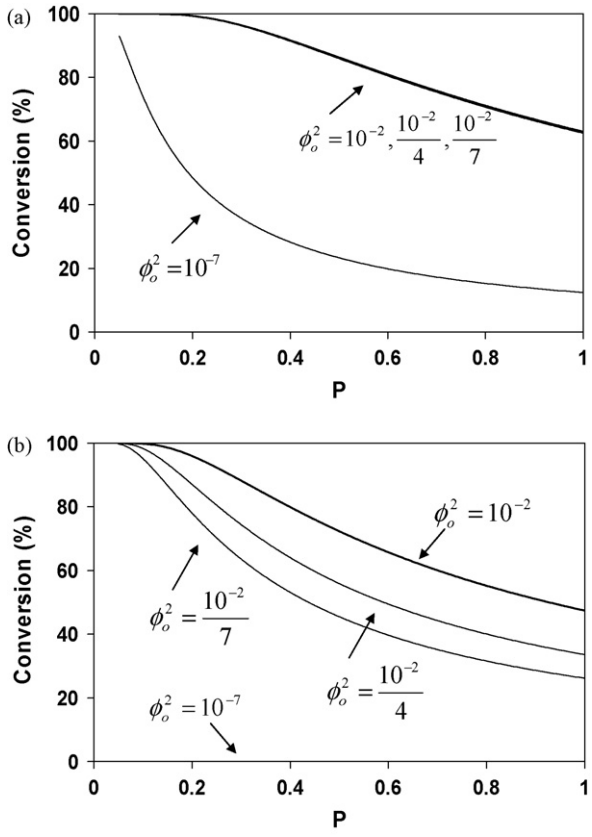

Fig. 17. Effect of space velocity (a) $T = 300\ ^\circ C$; (b) $T = 100\ ^\circ C$; monolith [for parameter values $T_o = 27\ ^\circ C$, $(R_\Omega/\delta_w)(D_{ei}/D_{mi}) = 1$, $E/RT_o = 30$].

temperatures, as previously mentioned the ignition (light-off) point moves to higher temperatures when the feed concentration of the reactant is increased [46]. To examine this effect quantitatively, we consider the simple case of a monolith in which both external and washcoat diffusional limitations can be neglected (i.e. homogeneous plug flow reactor). In this case, for a reaction whose rate is inversely proportional to the concentration, the conversion is given by

$$x = \begin{cases} 1 - \sqrt{1 - Da}, & Da \le 1 \\ 1, & Da > 1 \end{cases} \tag{26.a}$$

where

$$Da = Da_o \exp\left[\gamma\left(\frac{T - T_o}{T}\right)\right], \quad \gamma = \frac{E}{RT_o} \tag{26.b}$$

$$Da_o = \frac{Da_o^*}{C_f} \tag{26.c}$$

Here C_f is the dimensionless feed concentration and Da_o^* is the Damkohler number at the reference temperature and concentration. Fig. 18 shows the effect of feed concentration on conversion for a typical case ($Da_o^* = 0.1$, $\gamma = 30$, $T_o = 300$ K) for C_f values ranging from 0.1 to 1. We note that as the feed concentration increases by a factor of 10, the light-off point moves to the right by about 40 °C. These predictions (Fig. 18) are similar to the experiment results in Fig. 5a.

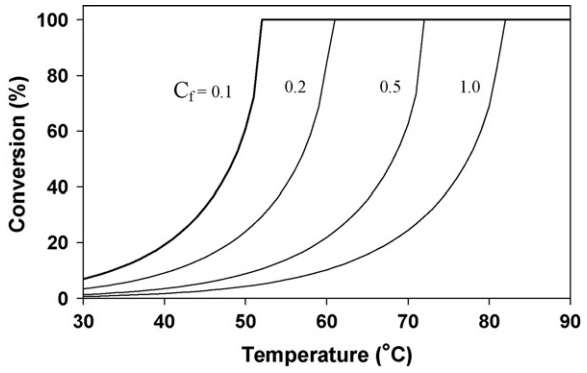

Fig. 18. Light-off curves for negative order kinetics for parameter values $T_o = 27\ ^\circ C$, $(R_\Omega/\delta_w)(D_{ei}/D_{mi}) = 1$, $E/RT_o = 30$, $Da_o^* = 0.1$.

4.5. NO + H_2 at higher temperatures

At temperatures exceeding 150 °C the product distribution shifts to a mixture of N_2 and NH_3. Their relative selectivities are dictated primarily by the temperature and the H_2/NO feed ratio according to global reactions (R2) and (R3). At higher temperature the rate of the surface decomposition of NO increases:

$$NO - Pt + Pt \leftrightarrow N - Pt + O - Pt \tag{S7}$$

In the low to moderate temperature range (150–250 °C) the N_2 selectivity exhibits a local maximum for $H_2/NO > 1.5$. To the right of the maximum the ammonia production increases with temperature; this suggests an energy barrier for ammonia production in the series of steps given by

$$N - Pt + H - Pt \leftrightarrow NH - Pt + Pt \tag{S8}$$

$$NH - Pt + H - Pt \leftrightarrow NH_2 - Pt + Pt \tag{S9}$$

$$NH_2 - Pt + H - Pt \leftrightarrow NH_3 - Pt + Pt \tag{S10}$$

$$NH_3 - Pt \leftrightarrow NH_3 + Pt \tag{S11}$$

Between 200 and 350 °C the two principal products are N_2 and NH_3. The relative selectivities follow closely the H_2/NO feed ratio. The relative coverages of nitrogen and hydrogen adspecies undoubtedly dictate the selectivities. Finally, at higher temperature (>350 °C) the ammonia produced from NO + H_2 decomposes under anaerobic conditions:

$$NH_3 \leftrightarrow 0.5N_2 + 1.5H_2 \tag{R6}$$

Previous studies of ammonia decomposition on Pt suggest a mechanistic sequence represented by the reverse of steps (S8)–(S11) [49]. The ammonia decomposition helps to explain the maximum in the ammonia selectivity under anaerobic conditions.

4.6. Aerobic NO + H_2 reaction system

The reaction pathways exhibited for the NO + H_2 + O_2 reaction system has some similar features (Fig. 6) to the anaerobic system in terms of the selectivities of N_2O, N_2, and

NH_3 (shown and modeled by Xu et al. [34]). The conversion versus temperature dependence has the usual sigmoidal dependence. At temperatures exceeding the light-off temperature, the conversion of NO is complete for $H_2/NO > 1$; for $H_2/NO < 1$ the conversion of H_2 is complete based on an overall hydrogen balance.

A sharp shift in product distribution occurs when the stoichiometric number, defined by Eq. (1), crosses unity. N_2O is a principal product at conditions of low temperature and lean conditions ($S_N > 1$) while N_2 and NH_3 are the main products under rich conditions ($S_N < 1$). An increase in the feed concentration of H_2 (S_N decrease) at a fixed temperature leads to an increase in the selectivity to NH_3 at the expense of N_2.

Under slightly lean conditions ($S_N = 1.1$) the ammonia selectivity is negligible with N_2 being the principal product. The NO_x conversion exhibits a maximum approaching 100%, but only over a narrow range of temperature, whereas for rich feeds the NO_x conversion reaches 100% at ignition and remains there over a wide temperature range. Similar results were reported previously by Burch et al. [47] for lean feeds. The existence of a NO conversion maximum has been reported for a variety of lean NO reduction studies [37,47,50]. Burch et al. [47] reported a maximum in NO conversion at light-off with propylene as the reductant under aerobic conditions. Xu et al. [34] reported a NO conversion maximum with a lean feed ($NO > H_2$) in the absence of gas phase O_2. That the conversion is nearly 100% speaks to the effectiveness of H_2 as a reductant as well as the high Pt loading in this study. At temperatures to the right of the maximum the selective reduction of NO by H_2 (reaction (R2)) competes with H_2 oxidation (R5). Insufficient hydrogen is available to react to form ammonia (R4). This is a result of an inadequate supply of H_2 to satisfy the stoiochiometric needs of N_2 formation reaction (R3) combined with an increasing rate of NO desorption.

4.7. NH_3 decomposition

The decomposition of ammonia is an important side reaction that contributes to reduced net production of ammonia at higher temperatures. Evidence for the decomposition pathway is the decline in ammonia selectivity at high temperatures encountered under anaerobic conditions (Fig. 4). The experiments carried out with the ammonia feed shown in Fig. 10b show the commencement of decomposition at about 400 °C. The NH_3 conversion decreases with increased feed rate (Fig. 10a) and increase H_2 in the feed (Fig. 10c). These results show that the reaction is slow compared to the other reactions and that it is inhibited by hydrogen. Loffler and Schmidt [49] also reported that H_2 hinders ammonia decomposition on polycrystalline Pt. This inhibition of NH_3 decomposition effects the performance of NO_x trap catalysts, to be reported in a future study.

4.8. NH_3 and NO oxidation

A second pathway for ammonia consumption is its oxidation by O_2. The experiments in which a mixture of NH_3 and O_2 was fed to the catalyst led to the formation of four principal N-containing products: N_2O, NO, NO_2, and N_2. The relevant overall reactions are:

$$NH_3 + 0.75O_2 \leftrightarrow 0.5N_2 + 1.5H_2 \quad (R7)$$

$$NH_3 + O_2 \leftrightarrow 0.5N_2O + 1.5H_2O \quad (R8)$$

$$NH_3 + 1.25O_2 \leftrightarrow NO + 1.5H_2O \quad (R9)$$

$$NO + 0.5O_2 \leftrightarrow NO_2 \quad (R10)$$

The data show the progression of N_2, N_2O, NO, NO_2 with increasing temperature. These results generally follow the NH_3/O_2 ratio. N_2 and N_2O are the main products at low temperature while NO is the primary product at high temperature. The maximum in the NO_2 selectivity is consistent with the reversibility of the NO oxidation chemistry [51,52]. The selectivity to NO also exhibits an interesting maximum at an intermediate O_2 concentration, more clearly seen in Fig. 12 for a fixed monolith temperature of 390 °C. At very low O_2 concentration (<1000 ppm) the main product is N_2, consistent with the decomposition of ammonia (R5) and reaction of H_2 with O_2 (R2); i.e., their sum is reaction (R7). As the O_2 concentration is increased the N_2 (NO) selectivity sharply decreases (increases). This suggests that the increased coverage of oxygen adatoms increases the rate of NO formation (reverse of (S7)). In addition, the reaction between surface NO and O species leads to NO_2 formation:

$$O_2 + 2Pt \leftrightarrow 2O - Pt \quad (S12)$$

$$NO - Pt + O - Pt \leftrightarrow NO_2 - Pt + Pt \quad (S13)$$

$$NO_2 - Pt \leftrightarrow NO_2 + Pt \quad (S14)$$

Weststrate et al. [53] observed no NO_2 formation on Pt (410) for stoichiometric feeds of O_2 and NH_3 ($O_2/NH_3 = 3/4$). This agrees well with our results for $O_2/NH_3 = 1$ in which no NO_2 was observed. Their results similarly favored N_2 formation for small O_2/NH_3 ratios.

4.9. NH_3 + NO

The third pathway for ammonia consumption is by its reaction with NO. The overall reaction under anaerobic conditions is given by

$$NH_3 + 1.5NO \leftrightarrow 1.25N_2 + 1.5H_2O \quad (R11)$$

Recent studies by Cumaranatunge et al. [17] show the importance of ammonia as a reductant of stored NO_x during NO_x storage and reduction. Understanding the relative steady-state reductive capabilities of H_2 versus NH_3 is important in assessing the more complex transient behavior of the NO_x trap. In the experiments with a feed containing an equimolar feed of NH_3 and NO (no H_2) the NH_3 conversion was approximately 67%, consistent with the stoichiometry of reaction (R11). As shown in Fig. 13, when H_2 was added the NH_3 conversion decreased linearly to zero at 500 ppm H_2 indicating a competitive rate effect. This suggests that the rate of NO reduction by H_2 (R3) is faster than by NH_3 (R11). The light-off temperatures for NO reduction by H_2 [34] and NH_3 (not shown

here) are approximately 80 and 180 °C, respectively, further revealing that H_2 is a more active reductant than NH_3 at low temperatures. The role of mass transport can also not be ruled out; the transport of H_2 to the catalyst surface is undoubtedly faster than that of NH_3.

4.10. Catalyst composition effects

The monolith catalyst data clearly show that Pt is the active component. The BaO component has some activity but is comparatively lower than that of Pt. The data shown in Figs. 2 and 3 for H_2/NO = 2.5 at 100 and 300 °C, respectively, reveal a monotonic dependence of the NO_x conversion on Pt loading for a fixed space velocity. The largest differences are between 0% Pt (B0), 0.32% Pt (B1), and 1.27% Pt (B2) catalysts. The insensitivity of conversion on Pt loading for the higher loading catalysts, 2.2% Pt (B3) and 3.71% Pt (B4), suggests a transition to a regime controlled by the feed rate. The decrease in NO_x conversion with space velocity underscores this point. The use of the simple reactor model accurately captured the trends with respect to loading as described earlier.

A comparison of the Pt-only and Pt/BaO catalysts with similar Pt loadings (A3 and B3) at 360 °C showed very little difference in terms of conversion and product distribution, indicating dominance by the active precious metal component [34]. On the other hand, the Ba-only (B0) catalyst exhibited moderate activity. The conversion versus space velocity plot at a catalyst temperature of 300 °C (Fig. 3) reveals that just 0.32% Pt (catalyst B1) increases significantly the space velocity range over which a high NO conversion can be achieved. For example, at 360,000 h^{-1} the NO conversion on the B1 catalyst is nearly 90% while on the B0 catalyst it is only 30%. Most of the results reported in this study were for the highly active A3 and B3 catalysts at 60,000 h^{-1} space velocity, conditions in which the overall rate was feed rate controlled. The Ba-only (B0) catalyst exhibited 100% NO conversion at 60,000 h^{-1}, decreasing to 80% conversion at 90,000 h^{-1} at 300 °C (Figs. 3a and 4a), but had negligible activity at 100 °C (Fig. 2a) in the same range of space velocities.

The Ba-only catalyst required pre-conditioning in order to exhibit a measurable activity. A redox cycle sustained between two different barium components such as barium hydroxide ($Ba(OH)_2$) and barium nitrite ($Ba(NO_2)_2$) can not explain the steady-state results, since cycling experiments (not shown here) on BaO (1s lean/rich and 2s lean/rich) between NO (500 ppm) balance N_2 and H_2 (1250 ppm) showed negligible reaction under similar conditions (temperature and H_2/NO ratio). A possible interpretation of the BaO/Al_2O_3 activity is that a short-lived NO intermediate that is formed on the BaO phase is reactive with co-fed H_2. That reaction does not occur under rapid cycling suggests that the coverage is low and its formation is reversible. Since the cycling experiments are longer than 1s the utilization of the intermediate is prevented and negligible NO conversion is observed. The Ba-only catalyst exhibited some selectivity differences compared to all of the Pt/Ba catalysts under the same conditions. Notably, the ammonia selectivity was lower at high H_2/NO feed ratios (>2) but slightly higher at low H_2/NO (<1). This suggests that kinetics of the reduction reactions may play a role. Further research is under going in our laboratory on the reactivity of barium with H_2 and NO and will be presented elsewhere.

5. Conclusions

A comprehensive study has been carried out to understand the effects of catalyst composition and operating conditions on steady-state NO reduction by H_2 with and without O_2. A series of $Pt/BaO/Al_2O_3$ monolith catalyst with varied Pt loading (0–3.71%) were compared. The results reveal that at 300 °C and under anaerobic conditions the reduction of NO is insensitive to Pt loading and only small amounts of Pt (0.32%) are required for complete conversion of NO at space velocities below 90,000 h^{-1}. At low temperatures (100 °C) and Pt loadings (<1.27%) the conversion and selectivities are strongly dependent on the Pt loading. The selectivity to N_2 has a maximum at low to moderate temperatures and a maximum in NH_3 selectivity occurs at about 400 °C. The product distribution is determined by the coupling of a complex set of coupled adsorption, desorption, and surface reactions and resulting surface coverages NO, N, H, and O.

At low temperature the aerobic NO–H_2 reaction system mainly produces N_2O and is positive (negative) order in H_2 (NO). The light-off temperature of the anaerobic NO–H_2 system is dictated by the kinetics as well as the Pt loading. Kinetic and theoretical analyses were carried out to support these observations. The kinetic analysis reveals that NO inhibits the NO–H_2 reaction (rate is negative order with respect to NO) while H_2 has a promotional effect. The light-off temperature is shown to be very sensitive to catalyst (Pt) loading in accordance with experimental observations.

The experiments show that NH_3 is a major product in the NO – H_2 – O_2 reaction system, especially under reducing conditions. Ammonia is a problematic byproduct during conventional NO_x storage and reduction (NSR). Understanding the conditions favorable for NH_3 formation and the interactions of NH_3 with the other species present is extremely important in order to help understand NO_x storage and reduction. The production of NH_3 increased with increasing Pt loading and H_2 concentration. A maximum in the selectivity to NH_3 was encountered at moderate to high temperatures. NH_3 was shown to be a major product under O_2 deficient conditions typical of the rich pulse in NSR, while N_2 and N_2O are the main products in the presence of O_2 (lean conditions). NH_3 oxidation ignited on Pt catalysts at 170–180 °C; in the ignited state a mixture of N_2, NO, NO_2 and N_2O was produced, the composition of which is sensitive to the NH_3/O_2 feed ratio and temperature. NO was found to selectively react with H_2 in the presence of NH_3 over the temperature range studied (40–500 °C). Experiments involving a feed containing H_2, NH_3, and NO reveal that H_2 is a much more effective reductant than NH_3. For temperatures exceeding 150 °C an equimolar mixture of the three components results in complete NO reduction by H_2 with negligible net conversion of NH_3. NH_3 was found to decompose above 330 °C in the absence of H_2 and small amounts of H_2

inhibit its decomposition. These findings have implications on regeneration of stored NO_x when H_2 is the reductant and is the focus of a future publication.

The selectivity versus temperature trends for the Pt/BaO and BaO catalysts had some common features but it is clear that different mechanisms are occurring. The BaO catalyst obtained up to 80% NO_x conversion at 300 °C while at 100 °C no reaction occurred. Under identical conditions (100 °C) the Pt-containing catalysts were active, achieving 13–100% conversion. In the presence of Pt the contribution of BaO was negligible due to the overwhelming activity of Pt.

The steady-state results from this study underpin our current effort in elucidating NO_x storage and reduction on Pt/BaO catalyst using H_2 as the reductant. In a future study we will utilize the results reported here to interpret trends during NO_x storage and reduction.

Acknowledgements

The work reported was supported by the U.S. DOE National Energy Technology Laboratory (DE-FC26-05NT42630). We also acknowledge BASF Catalysts LLC for providing the catalysts used in this study.

References

[1] K.S. Kabin, P. Khanna, R.L. Muncrief, V. Medhekar, M.P. Harold, Catal. Today 114 (1) (2006) 72–85.
[2] T.P. Kobylinski, B.W. Taylor, J. Catal. 33 (3) (1974) 376–384.
[3] H. Muraki, Y. Fujitani, Ind. Eng. Chem. Prod. Res. Dev. 25 (3) (1986) 414–419.
[4] J.C. Schlatter, K.C. Taylor, J. Catal. 49 (1) (1977) 42–50.
[5] H. Hirano, T. Yamada, K.I. Tanaka, J. Siera, B.E. Nieuwenhuys, Stud. Surf. Sci. Catal. 75 (1993) 345–357 (New Frontiers in Catalysis, Pt. A).
[6] H.G. Stenger Jr., J.S. Hepburn, Energy Fuels 1 (5) (1987) 412–416.
[7] W.C. Hecker, A.T. Bell, J. Catal. 88 (2) (1984) 289–299.
[8] W.C. Hecker, A.T. Bell, J. Catal. 92 (2) (1985) 247–259.
[9] G. Papapolymerou, A.G. Botis, A.D. Papargyris, X.D. Spiliotis, J. Mol. Catal. 84 (3) (1993) 267–281.
[10] R.L. Klimisch, K.C. Taylor, Ind. Eng. Chem. Prod. Res. Dev. 14 (1) (1975) 26–29.
[11] R.L. Klimisch, K.C. Taylor, Environ. Sci. Technol. 7 (2) (1973) 127–131.
[12] K. Otto, H.C. Yao, J. Catal. 66 (1) (1980) 229–236.
[13] H.C. Yao, M. Sieg, H.K. Plummer Jr., J. Catal. 59 (3) (1979) 365–374.
[14] R.L. Klimisch, G.J. Barnes, Environ. Sci. Technol. 6 (6) (1972) 543–548.
[15] J. Siera, B.E. Nieuwenhuys, H. Hirano, T. Yamada, K.I. Tanaka, Catal. Lett. 3 (2) (1989) 179–189.
[16] M. Shelef, H.S. Gandhi, Ind. Eng. Chem. Prod. Res. Dev. 11 (1) (1972) 2–11.
[17] L. Cumaranatunge, S.S. Mulla, A. Yezerets, N.W. Currier, W.N. Delgass, F.H. Ribeiro, J. Catal. 246 (1) (2007) 29–34.
[18] J.E. DeLaney, W.H. Manogue, Catal. Proc. Int. Congr., 5th 1 (1973) 267–278.
[19] H.C. Andersen, W.J. Green, D.R. Steele, J. Ind. Eng. Chem. (Washington, DC) 53 (1961) 199–204.
[20] M. Markvart, V. Pour, J. Catal. 7 (3) (1967) 279–281.
[21] M. Markvart, V. Pour, Chemicky Prumysl 19 (1) (1969) 8–12.
[22] J.A. Martin, M. Yates, P. Avila, S. Suarez, J. Blanco, Appl. Catal. B: Environ. 70 (1–4) (2007) 330–334.
[23] P.H. Mutin, A.F. Popa, A. Vioux, G. Delahay, B. Coq, Appl. Catal. B: Environ. 69 (1–2) (2006) 49–57.
[24] K. Otto, M. Shelef, J.T. Kummer, J. Phys. Chem. 74 (13) (1970) p2690.
[25] K. Otto, M. Shelef, Prep. Am. Chem. Soc., Div. Pet. Chem. 18 (3) (1973) 443–451.
[26] G.L. Bauerle, S.C. Wu, K. Nobe, Ind. Eng. Chem. Prod. Res. Dev. 14 (2) (1975) 123–130.
[27] K. Otto, M. Shelef, J.T. Kummer, J. Phys. Chem. 75 (7) (1971) 875–879.
[28] J.L. Gland, V.N. Korchak, J. Catal. 55 (3) (1978) 324–336.
[29] J.J. Ostermaier, J.R. Katzer, W.H. Manogue, J. Catal. 33 (3) (1974) 457–473.
[30] Edmondson, Gail, "Diesel Gets Cleaner and Greener," Business Week, 9 Feb 2006 http://www.businessweek.com/autos/content/feb2006/bw20060208_539996.htm.
[31] M. Hemingway, NO_x Remediation on Heavy-Duty Diesel Using On-Board Diesel Fuel Reforming, in: DEER Conference, Detroit, USA, 2006.
[32] H. Hu, Hybrid LNT/SCR NO_x Aftertreatment System for On-Highway Heavy-Duty Diesel Engines, in: DEER Conference, Detroit, USA, 2006.
[33] T. Morita, N. Suzuki, N. Satoh, K. Wada, H. Ohno, Study on Low NO_x Emission Control Using Newly Developed Lean NO_x Catalyst for Diesel Emissions, SAE, 2007,, p. 1–7.
[34] J. Xu, R. Clayton, V. Balakotaiah, M.P. Harold, Appl. Catal. B: Environ. 77 (2008) 395–408.
[35] P.B. Weisz, C.D. Prater, Advances in Catalysis, 6, Academic Press Inc., New York, N.Y., 1954, p. 143–96.
[36] M.P. Harold, M. Sheintuch, D. Luss, Ind. Eng. Chem. Res. 26 (4) (1987) 794–804.
[37] D.K. Captain, K.L. Roberts, M.D. Amiridis, Catal. Today 42 (1-2) (1998) 93–100.
[38] G. Pirug, H.P. Bonzel, J. Catal. 50 (1) (1977) 64–76.
[39] M. Gruyters, A.T. Pasteur, D.A. King, J. Chem. Soc., Faraday Trans. 92 (16) (1996) 2941–2950.
[40] F.V. Caballero, L. Vicente, Chem. Eng. J. (Amsterdam, Netherlands) 106 (3) (2005) 229–240.
[41] B.E. Nieuwenhuys, Adv. Catal. 44 (1999) 259–328.
[42] J. Siera, P. Cobden, K. Tanaka, B.E. Nieuwenhuys, Catal. Lett. 10 (5-6) (1991) 335–342.
[43] H. Hirano, T. Yamada, K.I. Tanaka, J. Siera, P. Cobden, B.E. Nieuwenhuys, Surf. Sci. 262 (1-2) (1992) 97–112.
[44] V. Medhekar, V. Balakotaiah, M.P. Harold, Catal. Today 121 (3-4) (2007) 226–236.
[45] J.L. Gland, E.B. Kollin, J. Catal. 68 (2) (1981) 349–354.
[46] M.P. Harold, M.E. Garske, J. Catal. 127 (2) (1991) 524–552.
[47] R. Burch, P.J. Millington, A.P. Walker, Appl. Catal. B: Environ. 4 (1994) 65–94.
[48] V. Balakotaiah, D.H. West, Chem. Eng. Sci. 57 (8) (2002) 1269–1286.
[49] D.G. Loffler, L.D. Schmidt, J. Catal. 41 (3) (1976) 440–454.
[50] K.S. Kabin, R.L. Muncrief, M.P. Harold, Catal. Today 96 (1-2) (2004) 79–89.
[51] M. Crocoll, S. Kureti, W. Weisweiler, J. Catal. 229 (2) (2005) 480–489.
[52] L. Olsson, B. Westerberg, H. Persson, E. Fridell, M. Skoglundh, B. Andersson, J. Phys. Chem. B 103 (1999) 10433–10439.
[53] C.J. Weststrate, J.W. Bakker, E.D.L. Rienks, C.P. Vinod, A.V. Matveev, V.V. Gorodetskii, B.E. Nieuwenhuys, J. Catal. 242 (1) (2006) 184–194.